LAWRENCE
LIVERMORE
NATIONAL
LABORATORY

LLNL-JRNL-824360

Protein-Mediated Actinide Mobility: A Potentially New Mechanism for the Migration of Radionuclides in the Environment.

G. Deblonde, J. Mattocks, A. B. Kersting, J. Cotruvo, M. Zavarin

July 10, 2021

Journal of the American Chemical Society

Disclaimer

Characterization of americium and curium complexes with the protein lanmodulin: a potential macromolecular mechanism for actinide mobility in the environment

Gauthier J.-P. Deblonde[1,2*], Joseph A. Mattocks[3], Huan Wang[4], Eric M. Gale[4], Annie B. Kersting[1,2], Mavrik Zavarin[1,2], and Joseph A. Cotruvo, Jr.[3*]

[1]*Physical and Life Sciences Directorate, Lawrence Livermore National Laboratory, Livermore, California 94550, United States*

[2]*Glenn T. Seaborg Institute, Lawrence Livermore National Laboratory, Livermore, California 94550, United States*

[3]*Department of Chemistry, The Pennsylvania State University, University Park, Pennsylvania 16802, United States*

[4]*Athinoula A. Martinos Center for Biomedical Imaging, Department of Radiology, Massachusetts General Hospital/Harvard Medical School, 149 Thirteenth Street, Charlestown, Massachusetts 02129, United States*

Abstract

Anthropogenic radionuclides, including long-lived heavy actinides such as americium and curium, represent the primary long-term challenge for management of nuclear waste. The potential release of these wastes into the environment necessitates understanding their interactions with biogeochemical compounds present in the environment. Here, we characterize the interactions between the heavy actinides, Am^{3+} and Cm^{3+}, and the natural lanthanide-binding protein, lanmodulin (LanM). LanM is produced abundantly by methylotrophic bacteria, including *Methylorubrum extorquens*, that are widespread in the environment. We determine the first stability constant for an Am^{3+}-protein complex (Am_3LanM) and confirmed the results with Cm_3LanM, indicating ~5-fold higher affinity than for lanthanides with most similar ionic radius, Nd^{3+} and Sm^{3+}, and making LanM the strongest known heavy actinide-binding protein. The protein's high selectivity over ^{243}Am's daughter nuclide ^{239}Np enables lab-scale actinide-actinide separations as well as provides insight into potential protein-driven mobilization for these actinides in the environment. The luminescence properties of the Cm^{3+}-LanM complex, and NMR studies of Gd^{3+}-LanM, reveal that lanmodulin-bound f-elements possess two coordinated solvent molecules across a range of metal ionic radii. We show under a wide range of environmentally relevant conditions that lanmodulin effectively outcompetes desferrioxamine B, a hydroxamate siderophore previously proposed to be important in trivalent actinide mobility. These results suggest that natural lanthanide-binding proteins such as lanmodulin may play important roles in speciation and mobility of actinides in the environment; it also suggests that protein-based biotechnologies may provide a new frontier in actinide remediation, detection, and separations.

Introduction

The nuclear age has brought about the release of synthetic actinide isotopes into the environment from weapon tests and wastes from research activities and nuclear reactors. The study of actinide complexation under environmentally relevant conditions has so far been limited to their interactions with mineral phases, small inorganic ions (e.g., carbonate/bicarbonate), small water-soluble organic chelators (e.g., acetate, citrate…), organic colloids (e.g. humic acid), or mineral organic colloids.[1–3] By contrast, metalloproteins have received little attention and very little is known about the behavior of actinides in the presence of these macrochelators that are ubiquitous in nature. Prior studies have focused on internal contamination with actinides and, as such, only concern mammalian proteins: transferrin[4–7], ferritin[8,9], fetuin[10–12], albumin[13], calmodulin[14,15], siderocalin[16,17], α-amylase[18,19] and ostepontin[20,21]. However, these proteins have evolved to bind common cations such as Fe^{3+} or Ca^{2+}, and they exhibit relatively low affinity for the actinide ions (**Table S1**). Moreover, besides the few studies mentioned above, prior works have been mainly dedicated to tetravalent actinides (Th^{4+}, Pu^{4+}) and uranyl (UO_2^{2+}) instead of heavy actinides, a situation that is likely due to the predominance of thorium, uranium, and plutonium in the nuclear energy sector. The high availability and low specific activities of the research isotopes involved (^{232}Th, ^{238}U, ^{242}Pu) also facilitate their study as opposed to americium and curium isotopes ($^{243/241}Am$ and $^{248/246/244}Cm$), which are much more hazardous and cost prohibitive (**Table S2**). Nevertheless, transplutonium elements, such as Am and Cm, represent a major challenge for countries willing to implement spent-fuel reprocessing strategies[22,23] as the presence of transplutonium elements significantly increases the toxicity of the nuclear waste during the first few thousand years.[24–26] As such, mechanisms that impact their chemical behavior and mobility in the environment must be better understood.[27] Transplutonium elements generally favor the +III oxidation state as their most stable, as do the lanthanides. Consequently, the recent discovery of

biological utilization of lanthanides[28,29] has opened new, as yet unexplored, possibilities for understanding actinide speciation in the environment.[30]

Within the last decade, lanthanides have been shown to be utilized as cofactors in metal- and pyrroloquinoline quinone-dependent alcohol dehydrogenases in methylotrophic bacteria that inhabit a range of environments – in soil and water[31–33], associated with plants[34], and even in volcanic mudpots[35]. Although related calcium-dependent enzymes also exist, the lanthanide-dependent ones have been proposed as the ancestral and most widespread of these enzymes[36], implying that lanthanide utilization is ubiquitous in environmental bacteria[37] and perhaps even in some higher organisms.[29] These discoveries stimulated further investigation to elucidate the mechanisms of lanthanide acquisition and handling in these organisms, which could inform efforts to extract, separate, and detect technologically important lanthanides. The first biomolecule to be identified and characterized in this search, which in turn led to identification of the first uptake system[34,38], is the highly selective lanthanide-binding protein, lanmodulin (LanM).[39] LanM homologs are broadly distributed in alpha- and gammaproteobacterial methylotrophs[39–41] that are found in soil, water, and associated with plants. While LanM is expressed in the bacteria in which it has been studied genetically in the absence of lanthanides, its transcript is strongly upregulated in bacteria exposed to light lanthanides, both *in vitro* and in plant-microbiome systems.[34,42] The protein itself is also abundant in whole-cell and partially purified lysates of *Methylorubrum extorquens*, which was how the protein was discovered in 2018.[39] Although its function has not been fully elucidated, it is encoded adjacent to a TonB-dependent transporter[39], and with a cluster that contains multiple genes involved in lanthanide uptake and periplasmic handling, strongly suggesting its function in these pathways.[34,38,43]

As the first characterized natural protein that has evolved to selectively bind trivalent lanthanides, our prior characterization of LanM has focused on understanding its interactions with the lanthanide series. LanM is a small, ~12 kDa protein that undergoes a conformational change from an unfolded state to a folded state in response to picomolar free concentrations of lanthanides.[39] Its complex with Y^{3+} has been structurally characterized, revealing a unique protein architecture consisting of two pairs of EF hands linked by unusually short helical regions.[44] Three of those EF hands bind lanthanides with picomolar affinity, whereas binding of all other metals tested to date, such as Ca^{2+}, Zn^{2+}, and Cu^{2+}, is hundreds of millions fold weaker and induces an incomplete conformational change.[38,39,45] As measured by CD spectroscopy to monitor the conformational transition, the protein exhibits highest affinity for the biologically relevant early lanthanides, La-Nd, with a decrease in apparent affinity to the right across the series.[38,39,45] However, the protein's metal recognition is complex. Comparison of apparent[39] and intrinsic[45] dissociation constants for lanthanides across the series suggests that the protein's conformational change is not equally coupled to all lanthanides; these values agree well for early lanthanides (particularly Nd), but diverge to either side. The similarities between the coordination chemistry of lanthanides and trivalent actinides suggest that lanmodulin would also be an exceptional chelator for actinides. Indeed, we recently posted a preprint[46] showing for the first time that LanM binds an actinide, the extremely rare but medically important actinium (Ac^{3+}), with 2-fold higher affinity than for La^{3+}, the lanthanide closest in ionic radius, and also >2-fold higher affinity relative to Y^{3+}. These results, in combination with the presence of LanM in numerous methylotrophs, prompted us to investigate LanM's interactions with the heavy actinides, which are more environmentally relevant and hazardous than naturally occurring actinium isotopes (which only exist at tracer levels and have short half-lives).[46]

In this manuscript, we use a variety of methods (including spectrophotometric titrations, steady-state and time-resolved luminescence) to characterize the stability and structure of the complexes of LanM with the heavy actinides, Am^{3+} and Cm^{3+}, revealing tighter binding than for lanthanides and Ac^{3+}. Characterization of the Cm^{3+} complex allows determination of the number of coordinated solvent molecules per site, showing similarities to the lanthanides across a range of ionic radii. Importantly, we also show that lanmodulin outcompetes the An^{3+}-binding siderophore desferrioxamine B (DFOB) for Cm^{3+} over a wide pH and concentration range, suggesting that LanM could play a more important role in actinide mobility in the environment than siderophores, which have been proposed as major species for complexing actinides in aquatic systems.[47–49] Our results 1) suggest that LanM may be a natural, macromolecular actinophore, 2) point to the environmental relevance of LanM and other similar proteins in actinide speciation in the environment, and 3) suggest new and preferential LanM-mediated separation methods for actinides.

Results and discussion

Complexation of americium and separation of neptunium using LanM. The binding of trivalent heavy actinides to LanM was first evaluated by spectrophotometry (**Figure 1**). The Am^{3+} ion exhibits a Laporte-forbidden 5f→5f absorbance band around 500 nm that is sharp and sensitive to its coordination environment. Upon sequential additions of LanM to an Am^{3+} solution at pH 5 (acetate buffer), the 5f→5f absorbance band progressively shifts from 504.0 nm to 505.2 nm, which is direct evidence that LanM binds to Am^{3+} in solution (**Figure 1A**). A minor feature also appears at 512-520 nm, similar to what has been observed for strong synthetic Am^{3+} chelating agents containing multiple carboxylate binding moieties.[50,51] While these absorbance features have been previously[50–52] used to study small-molecule complexes of Am^{3+}, they have not yet been

leveraged to study an americium-protein complex. To the best of our knowledge, spectroscopic techniques specific to americium have never been used to observed its direct binding to a protein. Only two cases of Am^{3+} binding to a macroligand have been documented. The first one concerns synthetic peptides (known as lanthanide binding tags, or LBTs), for which terbium luminescence was used as a marker during Am^{3+}/Tb^{3+} competitions at tracer-level concentrations.[53] The second case is the iron-transporting protein siderocalin,[17] which does not bind Am^{3+} directly, but instead under very specific conditions recognizes siderophore complexes of various metal ions, including f-elements. For the siderocalin-siderophore system, the protein luminescence band – a non-specific marker, independent of the nature of the metal – was used. In the case of LanM, the observed spectral variations are indicative of the formation of a polymetallic complex with a 3:1 stoichiometry, i.e., Am_3LanM (**Figure 1B**). These results are in excellent agreement with what we previously observed for the lanthanide ions.[39,45] It is important to note that LanM possesses four potential binding sites but, consistent with our observations with Ln^{3+}-LanM interactions,[39,44,45,54] the fourth site appears to exhibit too weak affinity to interact significantly with Am^{3+} under the conditions studied (pH 5.0, micromolar concentrations of LanM and Am^{3+}).

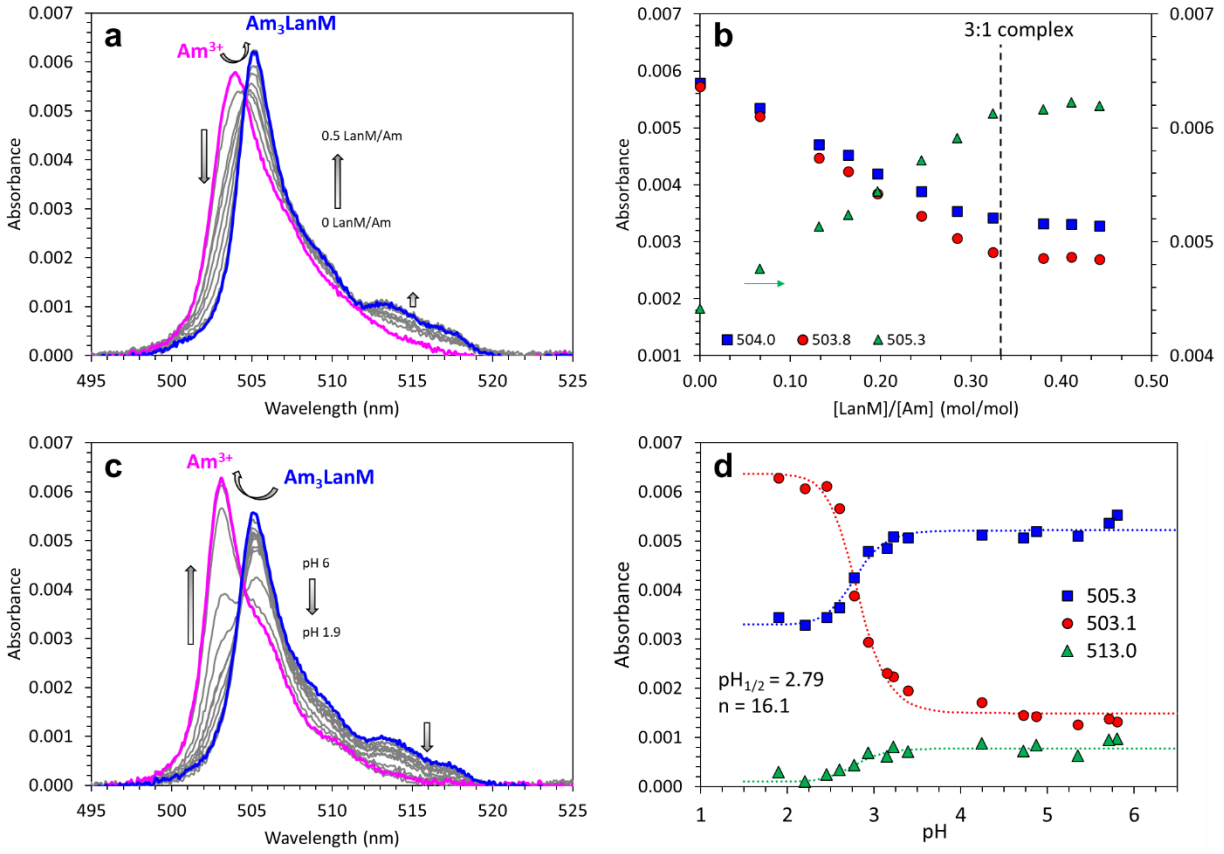

Figure 1. Americium binding to LanM, complex stoichiometry, and pH stability confirmed by absorbance spectrophotometry. (a) Representative spectrophotometric titration and observed spectral variations observed upon incremental additions of LanM to unbound Am^{3+} at pH 5.0. (b) Variation of the absorbance as a function of the ratio [LanM]/[Am] for the main spectral features. The vertical dotted line corresponds to the expected inflection point for the formation of Am_3LanM. [Am] = 15 µM. [LanM] = 0 to 6.9 µM. Buffer: 25 mM KCH_3COO, 75 mM KCl, pH 5.0. (c) Spectrophotometric titration of Am_3LanM as a function of pH and followed using the Am^{3+}-specific band at ~500 nm. (d) Change in the absorbance as a function of pH for the main spectral features (503.1, 505.3, and 513.0 nm). The dotted curves represent the best fits using the Hill equation. The average $pH_{1/2}$ and *n* values from three fits are displayed on the graph.

The binding of LanM to Am^{3+} was also tested under acidic conditions, since transuranic waste derived from nuclear fuel reprocessing activities are often acidic. Upon acidification of a Am_3LanM sample, no significant change is observed for the 5f→5f absorbance band until about pH 3; at pH below 3 the absorbance bands shift to 503.2 nm (**Figure 1C**), consistent with spectrum previously reported for uncomplexed Am^{3+} in acidic media.[51,55] Fitting of the spectral variations at three different wavelengths using the Hill equation (**Figure 1D**) yields a $pH_{1/2}$ value of 2.79±0.02. The absorbance spectra in the region that corresponds to the protein (<350nm; **Figure S1**) also show that the LanM releases the metal below pH 3, which is consistent with the changes

observed for the americium-specific absorbance band. Size-exclusion filtration experiments further confirmed the resilience of Am_3LanM under acidic conditions (**Figure S1**). Taken together, the results demonstrate that Am_3LanM can sustain acidic conditions as well as cover the circumneutral pH range encountered in natural aqueous streams. Am_3LanM can exist under a large range of pH conditions, similar to some of the strongest synthetic ligands that have been developed for trivalent actinides, such as the polyaminocarboxylates.[50,56,57]

Knowing that LanM was capable of binding americium in solution, we investigated its potential to influence the behavior of actinides belonging to the same nuclear decay chain. For instance, ^{243}Am decays to ^{239}Np (**Figure 2**) and these two elements are known to exhibit different oxidation states under environmental conditions, trivalent americium (Am^{3+}) and pentavalent neptunyl (NpO_2^+).[58,59] Moreover, we previously demonstrated that LanM has a unique selectivity for trivalent lanthanides ions over divalent and monovalent ions of the s- and d-blocks[38,39,45], but its selectivity relative to neptunium was unknown. Size-exclusion filtration experiments (**Figure 2**) suggest that LanM does not interact significantly with neptunium in solution under ambient conditions. Filtration of ^{243}Am/^{239}Np mixtures, initially at secular equilibrium, yields a complete separation of the two isotopes, with ^{243}Am being scavenged by LanM in the high-molecular-weight fraction and ^{239}Np passing through the filter in the low-molecular-weight fraction (**Figure S2**). LanM's selectivity and affinity toward Am^{3+} is so high that after a single filtration step, the ^{239}Np fraction does not contain a detectable amount of ^{243}Am, as confirmed by the decay profile (**Figure 2d**) and energy spectrum (**Figure S2**) of the low-molecular-weight fraction, which matches that of pure ^{239}Np. We estimate the radiopurity of the ^{239}Np produced via the one-step selective scavenging of ^{243}Am using LanM to be ≥99.5% (**Figure S3**). The radioactivity profile of the high-molecular-weight fraction (**Figure 2c**) is consistent with that of an ^{243}Am-rich fraction that has

been depleted from its ^{239}Np as its activity increases until it reaches a new secular equilibrium ^{243}Am-^{239}Np, hence further confirming the one-step separation of Np and Am induced by LanM.

Interestingly, this kind of LanM-driven separation between ^{243}Am and ^{239}Np does not require any adjustment of the redox conditions, use of highly acidic media, or liquid-liquid extraction steps, as is necessary in the usual laboratory preparations of purified neptunium solutions.[60] While this type of LanM-based isotope separation can be useful for rapid purification of ^{243}Am and ^{239}Np for heavy actinide research, it also raises the possibility of LanM as a highly selective trivalent actinide-binding protein in the environment. If such selective binding occurs in nature, it will yield a natural process for breaking the decay chain of certain heavy actinide isotopes with, for example, ^{243}Am being scavenged by LanM while the migration behavior of ^{239}Np (and of the rest of the decay chain: ^{239}Pu, ^{235}U…) would be controlled by the chemistry of the free ion. The same situation would apply for the main contributors of the long-term toxicity of the nuclear waste, namely ^{241}Am, whose first daughter is ^{237}Np (followed by ^{233}Pa and ^{233}U) and ^{244}Cm, which decays to ^{240}Pu and ^{236}U. Other relevant decay chains containing trivalent actinides (^{232}Th, $^{239/240/241/244}$Pu, $^{233/235/236}$U, $^{246/247/248}$Cm, $^{251/249}$Cf…) would also likely yield to natural separations of parent nuclides and products in the presence of LanM. The identification of natural ligands with combined high affinity and high selectivity for trivalent actinides, like LanM, may also help to elucidate apparent isotopic fractionation phenomena that have been observed[27] in the environment for ^{239}Pu and ^{240}Pu (which decays from ^{244}Cm).

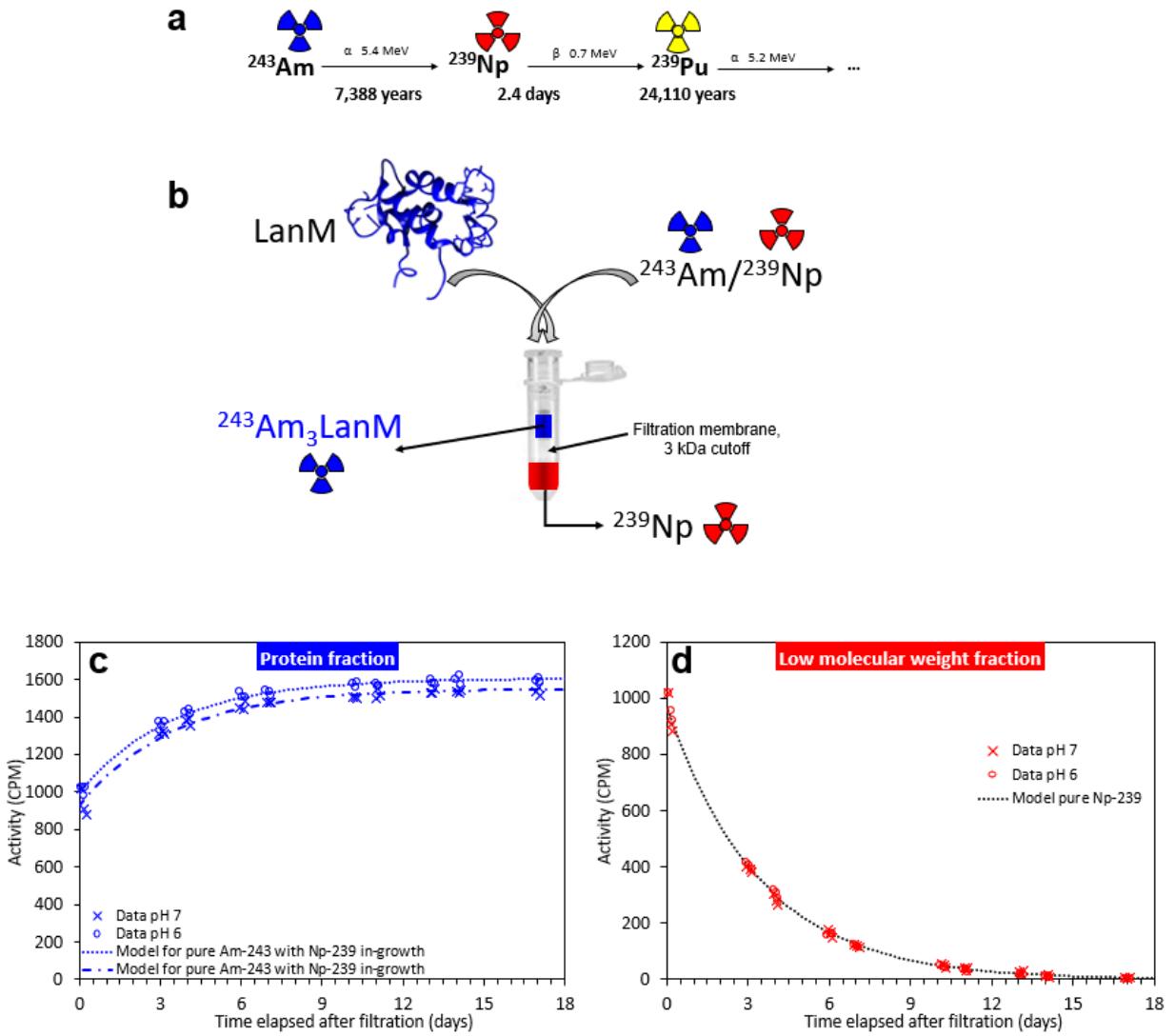

Figure 2. LanM enables the efficient sequestration of actinides, leading to decay chain break. (a) Beginning of the ^{243}Am decay chain. (b) Principle of the LanM-driven separation of actinides via size-exclusion filtration. The trivalent actinide (e.g., Am^{3+}) is selectively bound to LanM and cannot pass the filter's membrane. The other actinides (e.g., NpO_2^+) pass through the filter leading to the direct separation and break of the decay chain. (c) Radioactivity profile measured for protein fractions obtained after size-exclusion separation of ^{243}Am/^{239}Np samples (pH 6.0 and 7.0) initially at secular equilibrium, using C-terminally His_6-tagged LanM (^{His}LanM, see Methods). (d) Corresponding activity measured in the low-molecular-weight fraction. The dotted lines in the bottom panels correspond to the activity profiles expected for pure ^{239}Np or ^{243}Am (and its natural in-growth of ^{239}Np due to a new secular equilibrium), as indicated on the graphs. [^{His}LanM] = 10 µM. [Am-243] = 1 µM. Buffer: 25 mM HEPES, 75 mM KCl. Molecular weight cut-off = 3 kDa.

Taking advantage of the spectrophotometric properties of Am^{3+}, the formation constant of Am_3LanM was determined using ligand-competition titration with EDTA, analogously to our prior determination[45] of Ln_3-LanM stability constants. As shown in **Figure 3**, successive additions of EDTA to Am_3LanM trigger a progressive shift of the 5f→5f absorbance feature from 505.2 nm to

506.3 nm. The spectral variations indicate that EDTA and LanM compete for the binding to Am^{3+} as more than 5 equivalents of EDTA are needed to completely displace Am^{3+} from its LanM complex. The spectrum measured at high excess of EDTA in the 500 nm region is in excellent agreement with the spectrum reported by Griffiths et al.[61] for the Am-EDTA-H_2O system and we ascribe the corresponding species to $[AmEDTA]^-$. The titration results systematically show a single isosbestic point at 505.5 nm, which is consistent with an exchange reaction between two Am^{3+} complexes. Additionally, the ligand exchange reaction was also followed by monitoring another americium-specific band that is located at ~800 nm. This absorbance feature is rarely measured because its molar absorptivity is about ten times lower than the band at ~500 nm. Nonetheless, the spectral changes in this near-infrared region also indicate that LanM and EDTA compete for Am^{3+}, with the spectrum shifting from a broad band centered at 808 nm (Am_3LanM) to a doublet at 792 and 819 nm ($[AmEDTA]^-$). The absorbance spectra in the protein-specific region also corroborate the fact than LanM competes with small synthetic ligands such as EDTA. As the stability constant of $[AmEDTA]^-$ is known (log β_{11} = 16.9)[55,62], fitting of the spectrophotometric data in the three spectral windows allows determination of the formation constant for Am_3LanM. The experiments were performed with the untagged, wild-type protein (LanM) as well as with a version that includes a C-terminal hexahistidine tag (^{His}LanM – see the Materials section of the Methods), so that log β_{31} and K_d values could be directly compared with those previously characterized for $Ln_3{}^{His}$LanM complexes.[39,45] A log β_{31} value of 35.6±0.5 was obtained for Am_3LanM at pH 5.0, while a value of 34.0±0.5 was obtained for the ^{His}LanM variant. As LanM possesses three binding sites, these formation constants correspond to an average K_d per site of 1.3±0.7 pM for Am_3LanM and 4.5±1.3 pM for $Am_3{}^{His}$LanM at pH 5.0 (See Methods section for β_{31} to K_d conversion); these results are

consistent with our prior observation,[39] with the lanthanides, that K_ds for the His-tagged protein are ~2-fold higher than for the untagged protein.

Our results represent the first stability constant determination for an americium complex where Am^{3+} is directly bound to a protein, affording a unique perspective on the chemistry of trivalent actinides with a natural macrochelator. In fact, besides Am_3LanM, the only reaction constant involving Am^{3+} and a protein that has been reported is the association between the complex $[AmEnterobactin]^{3-}$ or $[Am343\text{-}LI(1,2\text{-}HOPO)]^{-}$ and siderocalin (K_d = 240 pM and 29,000 pM at pH 7.4, respectively, **Table S1**). Siderocalin is an iron-scavenger protein that recognizes the small-molecule siderophore complexes of various metals (Fe^{3+}, Ln^{3+}, An^{3+}, Pu^{4+}, Th^{4+}…) via siderophore-mediated interactions, but it is unable to bind to the metal ions directly; therefore, the observed reactions largely depend on the siderophore ligand rather than the metal ion. Despite the paucity of prior data on americium-protein complexes, the Am_3LanM complex can be compared to curium-protein species since Am^{3+} and Cm^{3+} are two adjacent actinides with very similar ionic radius (1.157 Å and 1.147 Å, when nine-coordinated[63]). **Table S1** lists the trivalent actinide-protein complexes that have been studied so far. The Am_3LanM complex is by far the most stable trivalent actinide-protein complex, with, for example, its K_d being at least 3 orders of magnitude stronger than that of Cm^{3+}-transferrin.

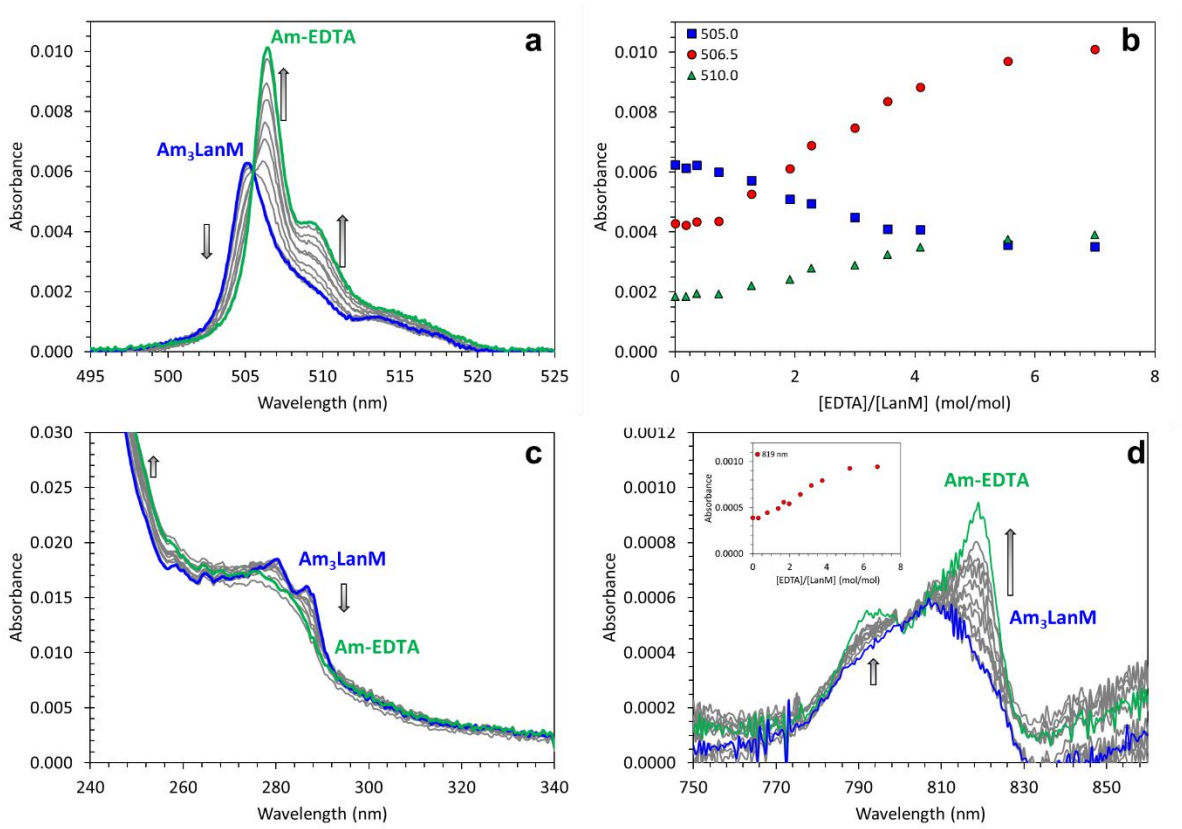

Figure 3. Stability constant determination for Am_3LanM. (a) Representative spectrophotometric titration of Am_3LanM using EDTA as competing ligand. [Am] = 15 µM. [LanM] = 6.6 µM. [EDTA] = 0 to 48 µM. Buffer: 25 mM KCH_3COO, 75 mM KCl, pH 5.0. (b) Change in absorbance as a function of ratio [EDTA]/[LanM] for the main spectral features (505, 506.5, and 510 nm). (c) Corresponding spectral changes observed in the protein-specific region of the spectrum (240-340 nm region). (d) Spectral changes observed for the Am^{3+}-specific band in the near-infrared region. Inset: absorbance profile at 819 nm as a function of the ratio [EDTA]/[LanM].

Interestingly, the affinity of LanM for Am^{3+} is higher than that of trivalent lanthanides (**Figure S4**). We previously determined the stability constants of ^{His}LanM with select lanthanide ions under the same conditions (pH 5.0) and the obtained log β_{31} value for $Nd_3{}^{His}$LanM was 32.0 (or K_d = 22.2 pM)[45], *i.e.* two orders of magnitude lower than for americium, yielding a 5-fold weaker K_d for Nd^{3+} versus the Am^{3+} complex. Log β_{31} values of 31.9 and 32.5 were also determined for $Pr_3{}^{His}$LanM and $Sm_3{}^{His}$LanM. Given that Am^{3+} has an ionic radius in the same range as Pr^{3+}, Nd^{3+}, and Sm^{3+} (1.176, 1.161, and 1.131 Å, respectively[63]), the results unequivocally demonstrate that LanM exhibits higher affinity for the actinides over the lanthanides of comparable ionic radius, a point supported by our recent comparison of Ac^{3+}- versus La^{3+}-bound LanM at

radiotracer levels.[46] The observation that the protein has slightly higher affinity for trivalent actinide ions over their lanthanide counterparts is reminiscent of prior characterization[50,51] of polyaminocarboxylate complexes. For small-molecule complexes, these experimental observations, in combination with density functional theory calculations, have been suggested to reflect slight differences in charge density and also a small degree of covalent interactions in the actinide bonds compared to the lanthanide bonds. However, it is not known at present whether such conclusions are applicable to large complexes like lanmodulin (where other phenomena also may be at play), which will be a topic of our future research. These results also suggest the possibility of efficient actinide-lanthanide separations using LanM in the frame of analytical chemistry. While advances in lanthanide biochemistry led to the discovery[39] of LanM as a natural, strong ligand for trivalent lanthanides, its preference for the actinides indicates that it is also a natural and very efficient actinide-binding protein.

Complexation of curium(III) by LanM. In order to further confirm the status of LanM as heavy actinide chelator, we also studied its interaction with curium(III) via fluorescence spectroscopy techniques. Owing to the electronic properties of Cm^{3+}, most of its compounds are luminescent when irradiated at ~400 nm, albeit with different intensities and unique spectral fingerprints. The complexation of Cm^{3+} by LanM was followed by measuring the emission spectra, excitation spectra, as well as luminescence lifetimes. As displayed in **Figure 4a-b**, upon sequential addition of LanM to Cm^{3+} solutions, a ~6-fold increase in the emission intensity was observed, indicative of the formation of a Cm^{3+}-LanM complex. The chelation of Cm^{3+} by LanM was also visible in the excitation spectra, where the main excitation peak shifts from 397 to 399 nm and increases by a factor of ~12. The brightness of Cm^{3+} in the presence of LanM also allows observation of the luminescence of Cm^{3+} via excitation at various wavelengths (**Figure S5** and **Figure S6**),

suggesting that such a protein-based system could be used for sensitive optical detection of actinides. In excellent agreement with the results obtained with Am_3LanM via independent techniques (*vide supra*), the intensities of the fluorescence emission and excitation peaks increase linearly with the ratio LanM/Cm and then plateaued once a ratio of 1/3 is reached, indicative of the formation of the polymetallic complex, Cm_3LanM (**Figure 4c-d)**.

The increase in emission intensity is accompanied by a peak shift from 595.5 nm (unbound Cm^{3+}) to 602.5 nm (Cm-LanM complex) as well as splitting of the peak in different Stark levels. The emission peak can be decomposed into four Gaussian peaks positioned at 585, 594, 602.5, and 610 nm, with relative intensities of 5%, 20%, 67%, and 8%, respectively (**Figure S7**). Interestingly, larger peak shifts relative to the free Cm^{3+} ion have been previously observed, notably with transferrin,[5,6,64] which has its main Stark level at ~620 nm. However, Cm_3LanM affords a unique insight into the class of curium-protein complexes because it is much more stable than the others previously reported, including its transferrin counterpart Cm_2Tf (**Table S1**); the results illustrate that there is no direct link between the strength of the Cm^{3+}-protein complexes and the position of their emission bands. Drobot and co-workers recently reported[15] the emission spectrum of Cm^{3+} in the presence of calmodulin (CaM) and the shape of the spectrum of the Cm-CaM species (likely Cm_4CaM by analogy with the observed stoichiometry of the Ln^{3+}-CaM species) looks relatively similar to the one of Cm_3LanM but its main peak position is at 605.2 nm, compared to 602.5 nm for Cm_3LanM. It is known that the K_d values of CaM with trivalent f-elements are in the micromolar range (hence ~6 orders of magnitude weaker than LanM[45]). This example also demonstrates that there is no direct correlation between peak positions and strength of the Cm^{3+}-protein complexes.

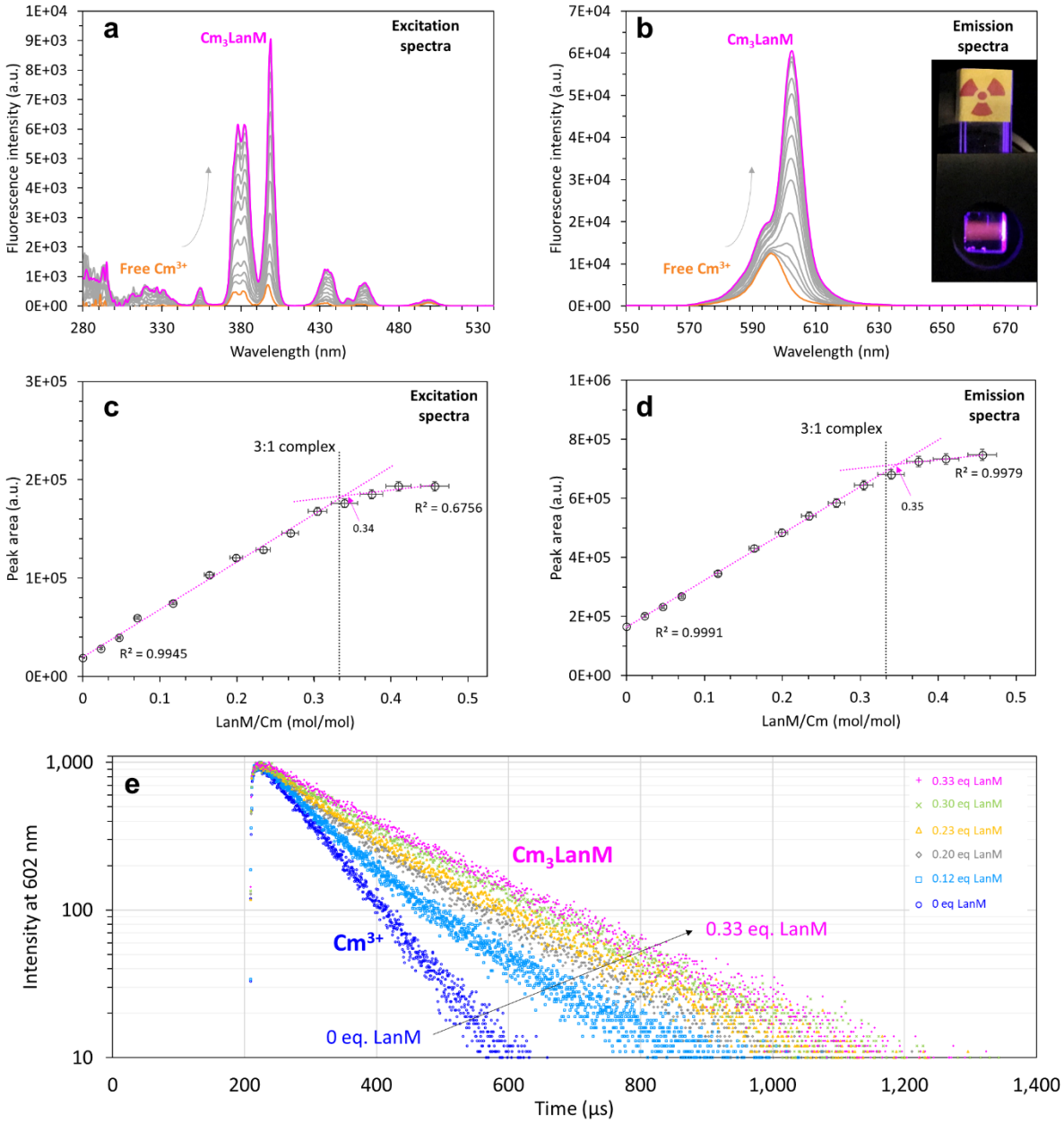

Figure 4. Complexation of Cm(III) by LanM. (a) Excitation spectra for Cm^{3+} measured as a function of the ratio [LanM]/[Cm]. [Cm] = 6 µM. [LanM] = 0 to 2.8 µM. λ_{em} = 602 nm. (b) Emission spectra for Cm^{3+} measured as a function of the ratio [LanM]/[Cm]. [Cm] = 6 µM. [LanM] = 0 to 2.8 µM. λ_{ex} = 399 nm. Inset: Picture of a Cm_3LanM sample under irradiation at 399 nm. (c) Calculated peak integral (280-560 nm) for the excitation spectra as a function of the ratio [LanM]/[Cm]. (d) Corresponding peak integral (550-680 nm) for the emission spectra. E) Curium fluorescence lifetime measured as a function of the ratio [LanM]/[Cm]. λ_{ex} = 399 nm. λ_{em} = 596 nm. Buffer: 25 mM KCH_3COO, 75 mM KCl, pH 5.0. For clarity, not all the lifetime measurements are displayed. See **Figure S10** and **Table S3** for additional time-resolved fluorescence results.

Monitoring of the luminescence properties of a Cm-LanM sample over a period of 5 days shows no significant change in its emission spectrum, excitation spectrum, or lifetime, indicating that the Cm_3LanM remains stable for an extended period of time (**Figure S8**). In terms of resilience

to acidic conditions, similar to what is observed for Am_3LanM, LanM remains bound to Cm^{3+} down to pH 2.5-3.0. As displayed in **Figure S9**, no significant change is observed in the excitation spectra or emission spectra over a broad pH range and both methods yield a $pH_{1/2}$ of 2.75±0.03. The evolution of the luminescence lifetime of the Cm-LanM samples as function of pH is also consistent with formation of a single species, *i.e.*, Cm_3LanM, from pH ~9 down to pH 2.75 (**Figure S10** and **Table S4**).

Leveraging the fluorescence properties of Cm^{3+}, we also determined the stability of Cm_3LanM via ligand-ligand competition titrations, using EDTA as a challenger, similar to the approach implemented for Am_3LanM but by monitoring the fluorescence emission and excitation spectra of the samples. Similar to the Am_3LanM case, about 6-8 equivalents of EDTA relative to ^{wt}LanM are needed to completely displace Cm_3LanM and form the $[CmEDTA]^-$ complex (**Figure S11**). In line with the spectral variations, the luminescence lifetime also shortens from 208±2 µs for Cm_3LanM (*vide infra*) to 147±2 µs in the presence of >6 equivalents of EDTA. This lifetime value is consistent with the one reported by Choppin et al.[65] for pure solutions of $[CmEDTA(H_2O)_x]^-$ (138±5 µs). Fitting of titration data using HypSpec[66] and considering the log β value previously reported for the $[CmEDTA]^-$ complex ($\log \beta_{11} = 17.4$)[62,67] yielded a formation constant, $\log \beta_{31}$, of 35.8±0.3 for Cm_3LanM at pH 5.0. This corresponds to an average K_d per site of 1.2±0.3 pM. The stability constant determined for $Cm_3{}^{wt}$LanM ($\log \beta_{31}$ of 35.8±0.3) is in excellent agreement with that measured for $Am_3{}^{wt}$LanM ($\log \beta_{31}$ of 35.6±0.5) under similar conditions but using an independent technique (*vide supra*). The similar stabilities of the curium and americium complexes are consistent with the almost-identical ionic radii of these two actinide cations (1.147 and 1.157 Å, respectively[63]). Taken together, the results obtained on Cm_3LanM and

Am_3LanM confirm that LanM forms robust complexes with the trivalent actinides and over a wide range of chemical conditions.

Solvent molecules coordinated to Cm^{3+} and Gd^{3+}-bound LanM. Luminescence lifetime measurements as a function of the ratio LanM/Cm are also evidence of the complexation of Cm^{3+} by LanM as a large increase in the lifetime was observed, from 84±2 µs for Cm^{3+} in acetate buffer without LanM to 208±2 µs once the Cm_3LanM is fully formed (**Figure 4e**). A luminescence lifetime of ~208 µs was consistently observed from pH ~9 down to pH ~3, indicating that the coordination environment of Cm^{3+} in Cm_3LanM remains similar over a broad pH range (**Figure S10, Table S3, and Table S4)**. The lifetime decay curves can be fitted adequately with a mono-exponential function indicating that the coordination environment of Cm^{3+} is relatively similar for the three metal-binding sites of Cm_3LanM. An empirical relationship has been developed by Kimura et al.[68] in order to calculate the number of coordinated water molecules present in Cm^{3+} complexes based on their fluorescence lifetime. This method has an uncertainty of ±0.5 H_2O molecules and, while it has been developed based on low-molecular-weight complexes, it is the only model available for Cm^{3+} complexes. Since the method was calibrated using carboxylate chelators (e.g., EDTA, CDTA, DTPA, NTA, oxalate, dipicolinate) we deemed it a suitable model for LanM and its carboxylate-containing binding sites. The 208 µs lifetime of Cm_3LanM corresponds to 2.2±0.5 water molecules. To further confirm the presence of H_2O molecules coordinated to Cm^{3+} in Cm_3LanM, we also measured its fluorescence lifetime in binary mixtures H_2O-D_2O, both by diluting a 100% H_2O sample of Cm_3LanM with D_2O, and by diluting a 97% D_2O sample of Cm_3LanM with H_2O. The fluorescence lifetime of Cm_3LanM was found to increase substantially as the content of D_2O increases and the results obtained from both methods are in excellent agreement (**Figure 5a**). The lifetime measured in 97% D_2O reaches 854 µs, and the

extrapolated value to 100% D_2O is 914 µs (**Figure 5b**). This result further confirms that solvent molecules are involved in the inner coordination sphere of Cm^{3+} in Cm_3LanM.

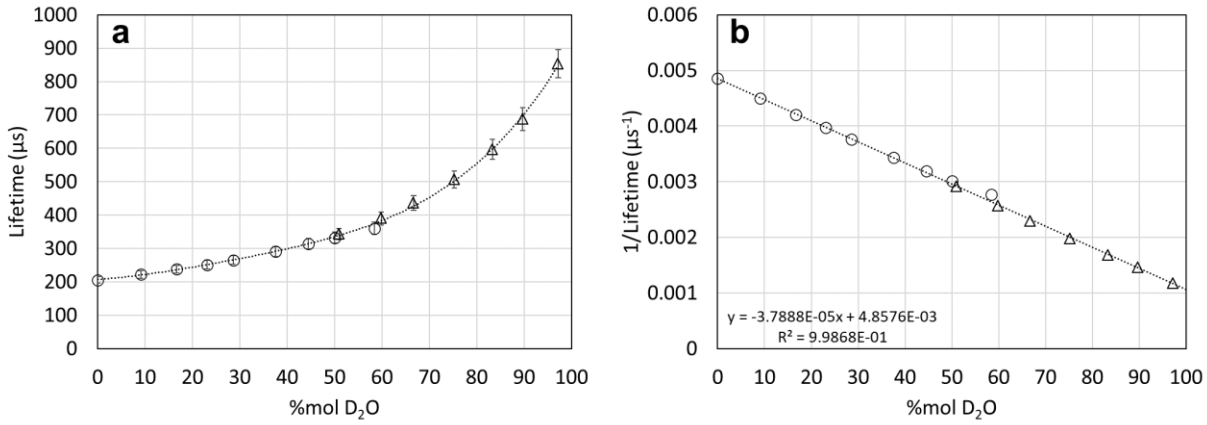

Figure 5. Luminescence lifetime of Cm^{3+} in Cm_3LanM measured in D_2O-H_2O mixtures. a) Direct lifetime values as a function of %D_2O. b) Linear correlation between inverse of the lifetime and %D_2O. The circles correspond to an H_2O sample diluted with D_2O. Conditions: 0.4 µM Cm^{3+}, 0.2 µM LanM, pH 7.0 (90 mM NaCl, 10 mM HEPES). The circles correspond to a 97.2% D_2O sample diluted with H_2O. Conditions: 2 µM Cm^{3+}, 1 µM LanM, pH 7.0 (90 mM NaCl, 10 mM HEPES). Error bars: ±5% (3σ). Excitation at 399 nm. Emission at 602 nm. See Table S5 for numerical values.

By comparison, Drobot et al.[15] observed via fluorescence spectroscopy and molecular dynamics simulations that, when substituting Ca^{2+} by Eu^{3+} or Cm^{3+} in calmodulin, ~3 water molecules coordinate the metal in the EF-hand 3 whereas the other three sites contain 2 water molecules. LanM and CaM share some structural similarities,[44] but the metal binding sites in LanM have a higher number of potential chelating moieties and are therefore more suitable for larger cations such as trivalent actinides. The NMR solution structure of Y^{3+}-LanM revealed[44] that each metal site possesses 6 potential proteinaceous ligands, including 5 carboxylates, but the denticity of each ligand and number of coordinated waters could not be determined by that method. Nonetheless, the abundance of protein residues and presence of water molecules in the first coordination sphere of Cm^{3+} in Cm_3LanM suggests that the water molecules may participate in the stabilization of the complex, perhaps via hydrogen bonding networks with at least one of the amino acid sidechains.

Interestingly, the number of coordinated water molecules per site for Cm^{3+}-LanM (i.e., 2.2±0.5) agrees well with a recent determination[54] for Tb^{3+}-LanM by luminescence lifetime measurements. We further interrogated the interactions of lanmodulin-chelated lanthanide ions through temperature-dependence ^{17}O NMR experiments performed on Gd^{3+}-LanM (**Figure S12**). For this experiment, we recorded the temperature dependence of the reduced T_2-relaxation rate of water ^{17}O (R_{2r} = the paramagnetically induced increased in $1/T_2$ normalized to mole fraction of water molecules directly coordinated to Gd^{3+}). For Gd^{3+}-LanM, two water co-ligands were inferred based on the Tb^{3+}-LanM system. We also note that the assumption of two water co-ligands yields R_{2r} values most consistent with values previously observed for Gd^{3+} complexes measured at the same field strength.[69–71] The data were fitted with an established four-parameter model of the Swift-Connick expressions describing two-site exchange, yielding the mean residency time at 310K (τ_m^{310}), the enthalpy of activation for water co-ligand exchange (ΔH), the longitudinal electronic relaxation time at 310K, and the T_{1e} activation energy (ΔE_{T1e}).[72] The fit yielded τ_m^{310} = 229 ± 53.6 ns, $\Delta H^{\ddagger}$ = 62.3 ± 11.1 kJ/mol, T_{1e} = 33.5 ± 7.63 ns, ΔE_{T1e} = -24.5 ±9.05 kJ/mol with χ^2 = 0.0011. These data are consistent with rapid water co-ligand exchange between Gd^{3+}-lanmodulin and bulk water, and support the observation of coordinated water molecules in the luminescence measurements.

Whereas Gd^{3+} and Tb^{3+} are not lanthanide ions that appear to be utilized by *M. extorquens* for growth,[38,73] the observation of 2 coordinated solvent molecules to Cm^{3+}, which has similar ionic radius to Nd^{3+}, suggests that at least 2 water molecules may be present at each site in LanM's complexes with the early lanthanides that do support growth. It is also of interest that LanM is able to stabilize complexes with 2 water molecules across a relatively wide range of ionic radii (~0.06 Å from Cm^{3+} to Tb^{3+},[63] assuming an identical coordination number, which remains to be tested).

Finally, the presence of these coordinated solvent molecules in the LanM complexes of actinides and lanthanides also leaves open the possibility of insertion of an additional ligand, similar to what is observed for transferrin and its various synergistic ions (carbonate, citrate, nitriloacetate…), that would serve to increase stability of LanM's Ln^{3+}/An^{3+} complexes even further.

Competition with environmentally relevant actinide chelators. Among the small ligands that have been studied for actinide binding in the environment, the siderophores have garnered significant attention since they are ubiquitous and are strong metal chelators. In particular, the tris-hydroxamate, desferrioxamine B (DFOB), has been extensively studied[47,74–76] and is often taken as a representative molecule of this class of ligands because it is widespread in nature, and it forms very strong complexes with plutonium[48,49,77] as well as with the trivalent lanthanides and actinides[78,79] (**Table S6**). It has been proposed that the DFOB complexes could represent as much as ~30% of the speciation of trivalent lanthanides in seawater, even if present at sub-nanomolar concentration.[79] In order to benchmark LanM's affinity for trivalent actinides, challenge experiments were performed between LanM and DFOB for the binding of Cm^{3+}. In a first set of experiments, Cm^{3+} was pre-complexed with LanM, forming Cm_3LanM, and challenged with DFOB. At pH 5.0, we found that DFOB is unable to break the Cm_3LanM complex, as confirmed by the lack of change in the emission spectra (**Figure 6**), excitation spectra (**Figure S13**), and lifetimes (**Figure S14**). Strikingly, even when using a ~3300-fold excess of DFOB relative to LanM, the Cm_3LanM remains completely formed. Moll et at. previously studied[78] the complexation of Cm^{3+} by DFOB and, based on the stability constants reported by the authors, the main complex between Cm^{3+} and DFOB that would form under our studied conditions (i.e., pH 5 and excess DFOB) would be $[CmH_2DFOB]^{2+}$ (**Figure S15**). Our results clearly indicate that Cm_3LanM is far more stable than $[CmH_2DFOB]^{2+}$. Similar experiments were also performed at

pH 7.0, 7.7, and 8.5 (**Figure 6** and **Figure S13**) where DFOB begins to successfully compete with LanM for binding to Cm^{3+}, albeit only partially. At pH 7.0, even with a large excess of DFOB present (~5,500 equivalents), 75% of the Cm^{3+} remains bound to LanM. At pH 7.7, additions of ~4,100 eq of DFOB relative to LanM only yields to ~50% displacement of Cm^{3+} from Cm_3LanM. At pH 8.5, DFOB can bind the majority of Cm^{3+} at the expense of LanM but at least ~2,400 equivalents are needed. It should be noted that such high concentrations of DFOB are very unlikely to occur in the environment. Modeling of the titration data using the emission spectra, excitation spectra, and the Cm-DFOB stability constants proposed by Moll et al.[78] yielded apparent formation constants for Cm_3LanM of 42.3±0.3 at pH 7.7 and 44.6±0.1 at pH 8.5, highlighting the high affinity of LanM for trivalent actinides. However, these values should be considered as tentative because multiple speciation models have been proposed for the trivalent f-element systems with DFOB and the speciation of these systems is still subject to debate (**Table S6**). Regardless, the results demonstrate that LanM readily outperforms multidentate hydroxamate chelators for the complexation of trivalent actinides under environmentally relevant conditions and over a wide range of pH values and concentrations.

In order to confirm these observations, the reverse experiments were also performed, starting from Cm^{3+} pre-complexed to DFOB and challenging it with LanM. A ratio of DFOB to Cm^{3+} of 500 equivalents was used for these experiments. As shown **Figure S16** and **Figure S17**, even under these favorable conditions for DFOB, LanM vastly outcompetes DFOB. At pH 7.0, the reaction is quantitative and only a stoichiometric amount of LanM ([LanM]/[Cm] = 1/3; [LanM]/[DFOB] = 1/1500) is needed to completely dissociate the Cm-DFOB complex and form Cm_3LanM. At pH 7.7, just ~1 µM LanM is required to completely retrieve Cm^{3+} from DFOB even in the presence of 1000 µM DFOB. At pH 8.5, ~50 µM LanM is needed to compete with the

1000 µM of DFOB but the ligand exchange reaction still occurs in favor of LanM. Taken together, the results not only demonstrate that the heavy actinide complexes of LanM would resist attack from strong chelators that are ubiquitous in nature, but they also show that LanM could vastly outcompete them, even from already formed complexes. This result suggests that even when LanM is released transiently by a bacterium it could significantly impact the biogeochemistry of actinides.

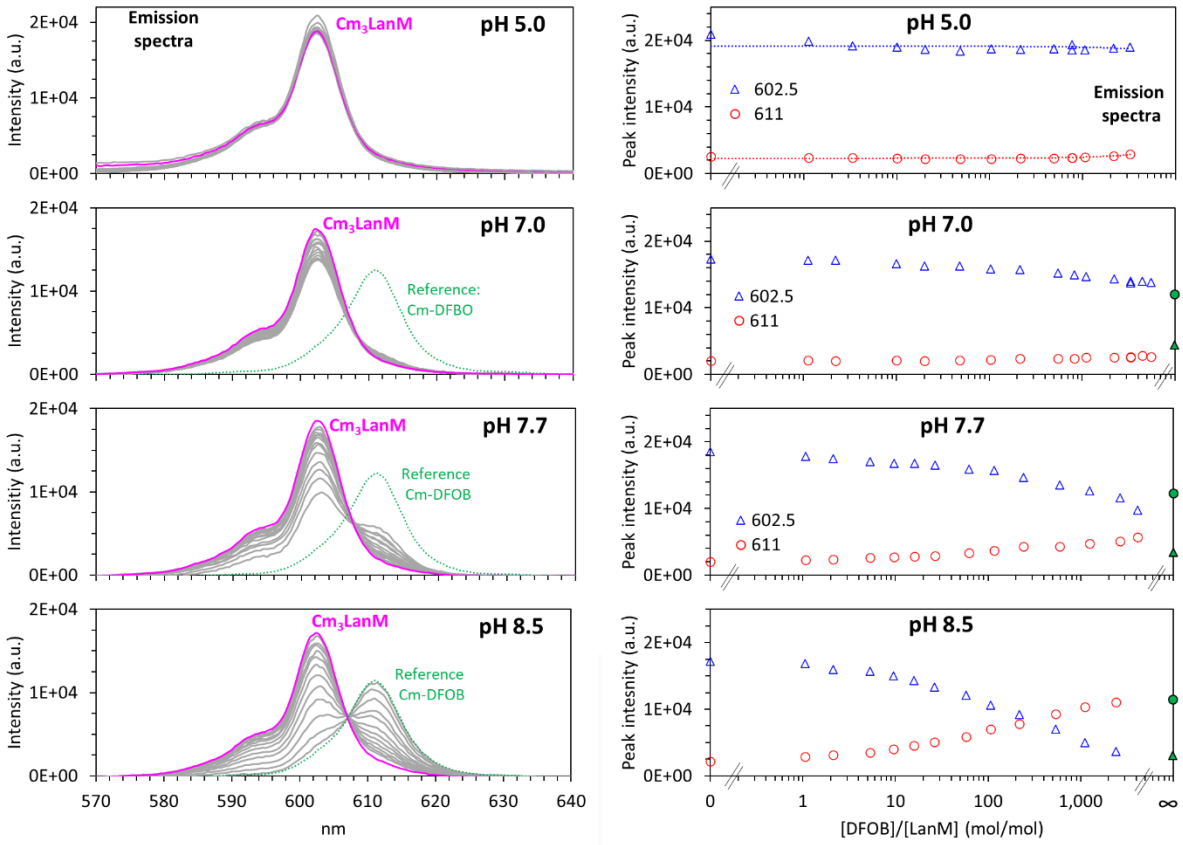

Figure 6. Competition between LanM and DFOB for the binding of Cm^{3+} followed by fluorescence spectroscopy. Cm_3LanM samples were challenged with a large excess of DFOB. Left: Emission spectra upon incremental additions of DFOB to Cm_3LanM and at different pH values (from top to bottom: pH 5.0, 7.0, 7.7, and 8.5). Each titration contains at least 12 spectra. Excitation at 399.0 nm. [Cm] = 2 µM. [LanM] = 1 µM. [DFOB] = 0 to up to 5,500 µM. The solid pink curve corresponds to Cm_3LanM. The green dotted curve corresponds to reference samples containing 2 µM Cm and 1,000 µM DFOB, in the same buffer and pH used for the titration. Right: Evolution of the intensity of the main emission bands (602.5 nm and 611.0 nm) as a function of the excess of DFOB, relative to LanM. The green triangles and circles on the right side of the graph correspond to the value measured for Cm-DFOB in the absence of LanM. The corresponding excitation spectra for all titrations are given in **Figure S13**. Reverse experiments were Cm-DFOB samples were challenged with LanM were also performed (See **Figure S16** and **Figure S17**).

Conclusions

Natural chelators that are ubiquitous in nature and effectively bind, transport, or immobilize trivalent actinides under environmentally conditions (i.e., actinophores), have been long sought. The understanding of lanthanide uptake in methylotrophs is still in its infancy and the present work represents an important step toward the extension of this research area to actinides. This study demonstrates that lanmodulin is not only the strongest trivalent actinide-binding protein ever characterized (outperforming any other metalloproteins by multiple orders of magnitude) but it also efficiently and selectively binds Am^{3+} and Cm^{3+} ions under a broad range of environmentally relevant conditions. LanM also outcompetes small chelators, such as the polyaminocarboxylates and the tris-hydroxamate siderophore DFOB, that are generally considered to play an important role in the mobility of radionuclides in the environment. This case study brings forward a potentially new mechanism for the biogeochemistry of actinides in the environment where the combined affinity and selectivity of LanM (and other similar proteins to be discovered), as well as its macromolecular nature could yield distinct complexation mechanisms for trivalent f-elements relative to other isotopes present in their decay chains. Additionally, the Am_3LanM and Cm_3LanM complexes of LanM display higher stability than the protein's natural substrates (lanthanides) raising the question whether microorganisms relying on LanM's machinery and lanthanoenzymes can also utilize actinides. Actinides have been proposed to have played a role in the origins of life,[80] and the proposal that lanthanide-dependent methanol dehydrogenases are ancestral enzymes in C_1 metabolism[36] may have made actinide-binding proteins and enzymes contributors to biology in ancient times and again today. These possibilities could apply both intracellularly and extracellularly. For example, secretion of a robust, high-affinity, f-element-binding protein like LanM to supplement putative small-molecule-based uptake mechanisms under certain conditions

would be analogous to copper uptake in methanotrophs, which appears to involve high-affinity small-molecule chalkophores as well as secreted copper-binding proteins.[81,82] Taken together, these results suggest that natural lanthanide-binding proteins such as lanmodulin represent a thus far underappreciated and understudied, but nonetheless important, part of the biogeochemistry of f-elements and also highlight how protein-based biotechnologies may facilitate remediation, detection, and potentially separations of lanthanides and heavy actinides.

Methods

Caution! *^{243}Am, ^{239}Np, and $^{248/246}$Cm, as well as their decay products, constitute serious health hazards because of their radioactive and chemical properties. Radiochemical experiments were conducted at LLNL in laboratories designed for the safe handling of short-lived and long-lived radioactive materials and associated waste.*

Materials. ^{243}Am samples were prepared by dilution of a primary standardized stock (Eckert & Ziegler, USA). Curium samples were prepared from a primary source (97% ^{248}Cm + 3% ^{246}Cm) from the LLNL inventory. Potassium chloride, sodium chloride, glycine, sodium acetate, potassium acetate, HEPES buffer, DFOB mesylate salt, EDTA, and all other non-radioactive chemicals were purchased from chemical providers (VWR and MilliporeSigma) and used as received. The Vivaspin® 500 protein concentrators were purchased from GE Healthcare and used according to the manufacturer's instructions. Untagged[83] and His-tagged LanM (^{His}LanM)[39] were purified as previously described. The untagged protein was used for all determinations, unless otherwise noted (i.e., Am/Np separation and $Am_3{}^{His}$LanM stability constant determination). All solutions were prepared using deionized water (≥ 18.2 MΩ.cm) purified by a reverse osmosis cartridge system (Thermo Scientific). All experiments were performed in a temperature-controlled room (22°C).

Radioanalysis. Liquid scintillation counting (LSC) was performed with a Perkin Elmer TriCarb 5110TR instrument equipped with an alpha/beta discriminator. Calibration was performed on a daily basis. Samples were diluted in UltimaGold^{TM} and results are background-corrected. Samples were counted long enough to maintain the statistical error (2σ) below 2.5%.

Fluorescence spectroscopy. Steady-state and time-resolved fluorescence spectra were measured with a FLS1000 spectrometer (Edinburgh Instruments) equipped with a double monochromator on the excitation arm and emission arm. A 450 W Xenon lamp was used as light source for the steady-state measurements and a 60 W microsecond flashlamp was using for lifetime measurements (MCS mode). Each lifetime decay curve contains 2,000 data points, with the maximum count per channel set to 1,000. The timespan of the acquisition was set so that the signal was measured until its return to background level. All fluorescence data were measured in sealed quartz cuvettes and the emission was collected at 90° relative to the excitation. Lifetimes were fit using the Fluoracle computer program (Edinburgh Instruments).

Size-exclusion filtration. Size exclusion experiments with ^{243}Am/^{239}Np samples were performed using centrifugal concentrators Vivaspin® 500 (GE Healthcare). These centrifugal concentrators contain a size exclusion membrane with a 3-kDa molecular weight cut-off. Samples containing ^{243}Am/^{239}Np and LanM were prepared in buffers of varied acidity, from pH 1 to ~7. The pH buffers contained 75 mM KCl and 25 mM of glycine, acetate, or HEPES and were pH-adjusted beforehand. The filters were rinsed with Milli-Q water and with the appropriate buffer at least 5 times prior to the introduction of the samples. After preparation of the samples and equilibration for 30 min, 400 µL of each sample were loaded in the filters, the filters were sealed, and then centrifuged for ~30 min at 12,000 rpm (15,294 ×*g*). The high-molecular-weight fraction (*i.e.*, protein fraction) was collected from the upper part of the centrifugal concentrators while the low-

molecular-weight fraction was collected from the lower part of the centrifugal concentrators. A representative aliquot of each fraction was taken out and analyzed by LSC immediately after filtration and periodically for at least ~20 days in order to follow the in-growth or decay of ^{239}Np. An instrument calibration and background measurement were performed before each LSC measurement.

UV-visible-NIR spectrophotometric titrations. Absorbance spectra of the Am(III) samples were measured using a high-performance Cary 6000i UV-vis-NIR spectrophotometer (Agilent Technologies). Samples were contained in sealed quartz cuvettes with a path length of 10 mm (10 mm × 4 mm cells) and the instrument was operated with narrow slits. Spectra were blank corrected by measuring the absorbance of the corresponding buffer prior to each titration. The initial sample volume was 400-500 µL. Instead of preparing separate samples at various LanM/EDTA ratios or separate samples in various buffers, sequential additions of LanM, EDTA, or acid were performed in order to minimize the radioactive material consumption and radiochemical exposure. For pH titration experiment, the pH value was measured between each addition. The duration between each addition was at least 15 min and each titration lasted at least 4 hours. The data were recorded in three distinct spectral windows: 230-350 nm for the LanM absorbance band, and 495-525 nm and 750-870 nm for Am(III). Two independent duplicates were performed for both the ^{WT}LanM and ^{His}LanM and the data fitting for stability constant determination was performed independently for each spectral window. The reported uncertainty on log β and K_d values corresponds to the standard deviation obtained from the 6 fitting procedures. All spectra were collected for dilution. The data treatment was performed with the computer program HypSpec[66] and has been detailed elsewhere.[45,84] The usual formalism used in biology for protein binding corresponds to dissociation constants "K_d," whereas global formation constants "β_{MLH}" are generally used to characterize

small-molecule complexes. As in our prior study of lanthanide-lanmodulin complexes,[45] here we report the equilibrium constants in terms of both averaged K_d per site and log β_{MHL} as defined by the following equations (charges are omitted for clarity):

$$\mathrm{MLanM} = \mathrm{M} + \mathrm{LanM} \;\; ; \;\; \mathrm{K_d^{11}} = \frac{1}{\beta_{11}} = \frac{[\mathrm{LanM}][\mathrm{M}]}{[\mathrm{MLanM}]} \qquad \text{Equation 1}$$

$$\mathrm{M_mLanM} = \mathrm{M} + \mathrm{M_{m-1}LanM} \;\; ; \;\; \mathrm{K_d^{m1}} = \frac{[\mathrm{M_{m-1}LanM}][\mathrm{M}]}{[\mathrm{M_mLanM}]} \qquad \text{Equation 2}$$

$$\beta_{31} = \frac{1}{\mathrm{K_d^{11}K_d^{21}K_d^{31}}} \qquad \text{Equation 3}$$

$$-\log \beta_{31} = \log \mathrm{K_d^{11}} + \log \mathrm{K_d^{21}} + \log \mathrm{K_d^{31}} = 3 \log \mathrm{K_d^{average}} \qquad \text{Equation 4}$$

$$\mathrm{K_d^{average}} = \frac{1}{\sqrt[3]{\beta_{31}}} \qquad \text{Equation 5}$$

Fluorescence spectroscopy titrations with competing chelators. Samples containing Cm^{3+} and LanM were prepared at pH 5.0 (Buffer: 25 mM KCH_3COO/CH_3COOH, 75 mM KCl), as well as pH 7.0, 7.7, and 8.5 (Buffer: 25 mM HEPES, 75 mM NaCl). The samples were equilibrated for at least 30 minutes. Their excitation spectra (λ_{em} = 602.5 nm), emission spectra (λ_{ex} = 399.0 nm), and luminescence lifetimes were measured. Detailed experimental conditions, with Cm^{3+}, LanM, and chelator concentrations, are given in the figure legends. Fresh stock solutions of the competing chelator (*i.e.*, EDTA or DFOB) were prepared in the corresponding buffer. Incremental additions of chelator were performed, and each addition was followed by measurement of the excitation spectrum, emission spectrum, and luminescence lifetime of the samples. The time between each addition of the competing chelator was at least 15 min. Measurements at longer intervals showed that the sample reached equilibrium within less than 15 min. Each titration lasted about 4 hours. For the DFOB experiments, the reverse titrations were also performed, starting with samples containing Cm^{3+} and DFOB and performing sequential additions of LanM. The resulting spectra

were corrected for the dilution induced by the sequential additions of chelator (the total added volume was typically <15% of the initial volume). For the determination of the stability constant of Cm_3LanM using EDTA as competitor, the experiment was performed in triplicate. The fitting of the titration data was performed using the computer program HypSpec and using the emission and excitation spectra, corresponding to a total of 6 datasets. The reported uncertainty corresponds to the overall standard deviation observed on the 6 procedures (experiment + fitting procedure). The stability constant determination experiments were performed under ambient atmosphere conditions using freshly prepared buffers. As the titrations consist of a ligand exchange reaction between LanM and EDTA, as they were performed at pH 5.0, and due to the much higher stability of the LanM and EDTA complexes relative to bicarbonate ones, the ambient concentration of bicarbonate does not significantly impact the metal speciation under these conditions.

Lifetime measurements in D_2O-H_2O mixtures. The influence of the deuterium/hydrogen ratio in the aqueous solvent on the fluorescence lifetime of Cm^{3+} in Cm_3LanM was determined in two ways. A sample containing 0.4 µM Cm^{3+} and 0.2 µM LanM was prepared in a 100% H_2O matrix (Buffer: 10 mM HEPES, 90 mM NaCl, pH 7.0) and was sequentially diluted with 99.9% D_2O (Sigma Aldrich), constituting a series of nine D_2O-H_2O binary mixtures, from 0% D_2O to 58.4% D_2O. Another sample containing 2.0 µM Cm^{3+} and 1.0 µM LanM in 97.2% D_2O was prepared independently (Buffer: 10 mM HEPES, 90 mM NaCl, pH 7.0). The 97.2% D_2O sample was then sequentially diluted using a 100% H_2O buffer, creating seven D_2O-H_2O mixtures, from 97.2% D_2O to 51.0% D_2O. For each mixture, the excitation and emission spectra were measured to verify that the Cm_3LanM was formed, and the lifetime was measured (λ_{ex} = 399.0 nm, λ_{em} = 602.5 nm). Each lifetime measurement contained 2,000 data points and had a maximum count per channel set

to 1,000. Lifetimes were fit using the Fluoracle computer program (Edinburgh Instruments). Single exponential decay was observed for the 16 D_2O-H_2O mixtures.

^{17}O NMR. Samples for ^{17}O NMR comprised 0.7 mM Gd^{3+}-lanmodulin (2.1 mM Gd^{3+}) in 20 mM MOPS, 100 mM KCl, pH 7.4, enriched with a small amount of $H_2{}^{17}O$. The transverse (T_2) relaxation times of ^{17}O at 11.7T were estimated from the full-width at half-height ($\Delta\nu_{1/2}$) of the ^{17}O NMR linewidth ($T_2 \sim (\pi\Delta\nu_{1/2})^{-1}$ at temperatures ranging from 298 to 353 K.[85] Reduced relaxation rates (R_{2r}) were calculated by dividing the Gd^{3+} induced increase in $1/T_2$ relative to that observed for the apoprotein divided by the mole fraction of coordinated water molecules. This data was plotted against reciprocal temperature (1000/T (K^{-1})) and fit to a four-parameter model as described previously.[72] The Gd-O hyperfine coupling constant, $A/\hbar$, was assumed to be -3.79 x 10^6 rad/s.[86]

References

(1) Geckeis, H.; Lützenkirchen, J.; Polly, R.; Rabung, T.; Schmidt, M. Mineral–Water Interface Reactions of Actinides. *Chem. Rev.* **2013**, *113* (2), 1016–1062. https://doi.org/10.1021/cr300370h.

(2) Geckeis, H.; Rabung, T. Actinide Geochemistry: From the Molecular Level to the Real System. *Journal of Contaminant Hydrology* **2008**, *102* (3), 187–195. https://doi.org/10.1016/j.jconhyd.2008.09.011.

(3) Kersting, A. B.; Efurd, D. W.; Finnegan, D. L.; Rokop, D. J.; Smith, D. K.; Thompson, J. L. Migration of Plutonium in Ground Water at the Nevada Test Site. *Nature* **1999**, *397* (6714), 56–59. https://doi.org/10.1038/16231.

(4) Jensen, M. P.; Gorman-Lewis, D.; Aryal, B.; Paunesku, T.; Vogt, S.; Rickert, P. G.; Seifert, S.; Lai, B.; Woloschak, G. E.; Soderholm, L. An Iron-Dependent and Transferrin-Mediated Cellular Uptake Pathway for Plutonium. *Nat Chem Biol* **2011**, *7* (8), 560–565. https://doi.org/10.1038/nchembio.594.

(5) Sturzbecher-Hoehne, M.; Goujon, C.; Deblonde, G. J.-P.; Mason, A. B.; Abergel, R. J. Sensitizing Curium Luminescence through an Antenna Protein To Investigate Biological Actinide Transport Mechanisms. *J. Am. Chem. Soc.* **2013**, *135* (7), 2676–2683. https://doi.org/10.1021/ja310957f.

(6) Bauer, N.; Fröhlich, D. R.; Panak, P. J. Interaction of Cm(III) and Am(III) with Human Serum Transferrin Studied by Time-Resolved Laser Fluorescence and EXAFS Spectroscopy. *Dalton Trans.* **2014**, *43* (18), 6689–6700. https://doi.org/10.1039/C3DT53371A.

(7) Adam, N.; Trumm, M.; Smith, V. C.; MacGillivray, R. T. A.; Panak, P. J. Incorporation of Transuranium Elements: Coordination of Cm(III) to Human Serum Transferrin. *Dalton Trans.* **2018**, *47* (41), 14612–14620. https://doi.org/10.1039/C8DT02915F.
(8) Auwer, C. D.; Llorens, I.; Moisy, P.; Vidaud, C.; Goudard, F.; Barbot, C.; Solari, P. L.; Funke, H. Actinide Uptake by Transferrin and Ferritin Metalloproteins. *Radiochimica Acta* **2005**, *93* (11), 699–703. https://doi.org/10.1524/ract.2005.93.11.699.
(9) Zurita, C.; Tsushima, S.; Bresson, C.; Cortes, M. G.; Solari, P. L.; Jeanson, A.; Creff, G.; Auwer, C. D. How Does Iron Storage Protein Ferritin Interact with Plutonium (and Thorium)? *Chemistry – A European Journal* **2021**, *27* (7), 2393–2401. https://doi.org/10.1002/chem.202003653.
(10) Basset, C.; Averseng, O.; Ferron, P.-J.; Richaud, N.; Hagège, A.; Pible, O.; Vidaud, C. Revision of the Biodistribution of Uranyl in Serum: Is Fetuin-A the Major Protein Target? *Chem. Res. Toxicol.* **2013**, *26* (5), 645–653. https://doi.org/10.1021/tx400048u.
(11) Younes, A.; Creff, G.; Beccia, M. R.; Moisy, P.; Roques, J.; Aupiais, J.; Hennig, C.; Solari, P. L.; Auwer, C. D.; Vidaud, C. Is Hydroxypyridonate 3,4,3-LI(1,2-HOPO) a Good Competitor of Fetuin for Uranyl Metabolism? *Metallomics* **2019**, *11* (2), 496–507. https://doi.org/10.1039/C8MT00272J.
(12) Vidaud, C.; Miccoli, L.; Brulfert, F.; Aupiais, J. Fetuin Exhibits a Strong Affinity for Plutonium and May Facilitate Its Accumulation in the Skeleton. *Sci Rep* **2019**, *9* (1), 17584. https://doi.org/10.1038/s41598-019-53770-6.
(13) Ali, M.; Kumar, A.; Kumar, M.; Pandey, B. N. The Interaction of Human Serum Albumin with Selected Lanthanide and Actinide Ions: Binding Affinities, Protein Unfolding and Conformational Changes. *Biochimie* **2016**, *123*, 117–129. https://doi.org/10.1016/j.biochi.2016.01.012.
(14) Seeger, P. A.; Rokop, S. E.; Palmer, P. D.; Henderson, S. J.; Hobart, D. E.; Trewhella, J. Neutron Resonance Scattering Shows Specific Binding of Plutonium to the Calcium-Binding Sites of the Protein Calmodulin and Yields Precise Distance Information. *J. Am. Chem. Soc.* **1997**, *119* (22), 5118–5125. https://doi.org/10.1021/ja9633124.
(15) Drobot, B.; Schmidt, M.; Mochizuki, Y.; Abe, T.; Okuwaki, K.; Brulfert, F.; Falke, S.; Samsonov, S. A.; Komeiji, Y.; Betzel, C.; Stumpf, T.; Raff, J.; Tsushima, S. Cm3+/Eu3+ Induced Structural, Mechanistic and Functional Implications for Calmodulin. *Phys. Chem. Chem. Phys.* **2019**, *21* (38), 21213–21222. https://doi.org/10.1039/C9CP03750K.
(16) Deblonde, G. J.-P.; Sturzbecher-Hoehne, M.; Rupert, P. B.; An, D. D.; Illy, M.-C.; Ralston, C. Y.; Brabec, J.; de Jong, W. A.; Strong, R. K.; Abergel, R. J. Chelation and Stabilization of Berkelium in Oxidation State +IV. *Nature Chemistry* **2017**, *9* (9), 843–849. https://doi.org/10.1038/nchem.2759.
(17) Allred, B. E.; Rupert, P. B.; Gauny, S. S.; An, D. D.; Ralston, C. Y.; Sturzbecher-Hoehne, M.; Strong, R. K.; Abergel, R. J. Siderocalin-Mediated Recognition, Sensitization, and Cellular Uptake of Actinides. *PNAS* **2015**, *112* (33), 10342–10347. https://doi.org/10.1073/pnas.1508902112.
(18) Barkleit, A.; Heller, A.; Ikeda-Ohno, A.; Bernhard, G. Interaction of Europium and Curium with Alpha-Amylase. *Dalton Trans.* **2016**, *45* (21), 8724–8733. https://doi.org/10.1039/C5DT04790K.
(19) Barkleit, A.; Wilke, C.; Heller, A.; Stumpf, T.; Ikeda-Ohno, A. Trivalent F-Elements in Human Saliva: A Comprehensive Speciation Study by Time-Resolved Laser-Induced Fluorescence Spectroscopy and Thermodynamic Calculations. *Dalton Trans.* **2017**, *46* (5), 1593–1605. https://doi.org/10.1039/C6DT03726G.
(20) Qi, L.; Basset, C.; Averseng, O.; Quéméneur, E.; Hagège, A.; Vidaud, C. Characterization of UO22+ Binding to Osteopontin, a Highly Phosphorylated Protein: Insights into Potential Mechanisms of Uranyl Accumulation in Bones†. *Metallomics* **2014**, *6* (1), 166–176. https://doi.org/10.1039/c3mt00269a.
(21) Szyrwiel, Ł.; Liauchuk, V.; Chavatte, L.; Lobinski, R. In Vitro Induction and Proteomics Characterisation of a Uranyl–Protein Interaction Network in Bovine Serum†. *Metallomics* **2015**, *7* (12), 1604–1611. https://doi.org/10.1039/c5mt00207a.

(22) Modolo, G.; Geist, A.; Miguirditchian, M. 10 - Minor Actinide Separations in the Reprocessing of Spent Nuclear Fuels: Recent Advances in Europe. In *Reprocessing and Recycling of Spent Nuclear Fuel*; Taylor, R., Ed.; Woodhead Publishing Series in Energy; Woodhead Publishing: Oxford, 2015; pp 245–287. https://doi.org/10.1016/B978-1-78242-212-9.00010-1.
(23) Chapron, S.; Marie, C.; Arrachart, G.; Miguirditchian, M.; Pellet-Rostaing, S. New Insight into the Americium/Curium Separation by Solvent Extraction Using Diglycolamides. *Solvent Extraction and Ion Exchange* **2015**, *33* (3), 236–248. https://doi.org/10.1080/07366299.2014.1000792.
(24) Ewing, R. C. Nuclear Waste Forms for Actinides. *PNAS* **1999**, *96* (7), 3432–3439.
(25) Geckeis, H.; Zavarin, M.; Salbu, B.; Lind, O. C.; Skipperud, L. Chapter 25: Environmental Chemistry of Plutonium. In *Plutonium Handbook*; American Nuclear Society, 2019.
(26) *Status of Minor Actinide Fuel Development*; Nuclear Energy Series; INTERNATIONAL ATOMIC ENERGY AGENCY: Vienna, 2010.
(27) Kurosaki, H.; Kaplan, D. I.; Clark, S. B. Impact of Environmental Curium on Plutonium Migration and Isotopic Signatures. *Environ. Sci. Technol.* **2014**, *48* (23), 13985–13991. https://doi.org/10.1021/es500968n.
(28) Daumann, L. J. Essential and Ubiquitous: The Emergence of Lanthanide Metallobiochemistry. *Angewandte Chemie International Edition* **2019**, *58* (37), 12795–12802. https://doi.org/10.1002/anie.201904090.
(29) Cotruvo, J. A. Jr. The Chemistry of Lanthanides in Biology: Recent Discoveries, Emerging Principles, and Technological Applications. *ACS Cent. Sci.* **2019**, *5* (9), 1496–1506. https://doi.org/10.1021/acscentsci.9b00642.
(30) Deblonde, G. J.-P.; Kersting, A. B.; Zavarin, M. Open Questions on the Environmental Chemistry of Radionuclides. *Commun Chem* **2020**, *3* (1), 1–5. https://doi.org/10.1038/s42004-020-00418-6.
(31) Nakagawa, T.; Mitsui, R.; Tani, A.; Sasa, K.; Tashiro, S.; Iwama, T.; Hayakawa, T.; Kawai, K. A Catalytic Role of XoxF1 as La3+-Dependent Methanol Dehydrogenase in Methylobacterium Extorquens Strain AM1. *PLOS ONE* **2012**, *7* (11), e50480. https://doi.org/10.1371/journal.pone.0050480.
(32) Wehrmann Matthias; Billard Patrick; Martin-Meriadec Audrey; Zegeye Asfaw; Klebensberger Janosch; Zhang Xinning; Newman Dianne K. Functional Role of Lanthanides in Enzymatic Activity and Transcriptional Regulation of Pyrroloquinoline Quinone-Dependent Alcohol Dehydrogenases in Pseudomonas Putida KT2440. *mBio* **2017**, *8* (3), e00570-17. https://doi.org/10.1128/mBio.00570-17.
(33) Groom, J. D.; Ford, S. M.; Pesesky, M. W.; Lidstrom, M. E. A Mutagenic Screen Identifies a TonB-Dependent Receptor Required for the Lanthanide Metal Switch in the Type I Methanotroph "Methylotuvimicrobium Buryatense" 5GB1C. *Journal of Bacteriology* **2019**, *201* (15), e00120-19. https://doi.org/10.1128/JB.00120-19.
(34) Ochsner, A. M.; Hemmerle, L.; Vonderach, T.; Nüssli, R.; Bortfeld-Miller, M.; Hattendorf, B.; Vorholt, J. A. Use of Rare-Earth Elements in the Phyllosphere Colonizer Methylobacterium Extorquens PA1. *Molecular Microbiology* **2019**, *111* (5), 1152–1166. https://doi.org/10.1111/mmi.14208.
(35) Pol, A.; Barends, T. R. M.; Dietl, A.; Khadem, A. F.; Eygensteyn, J.; Jetten, M. S. M.; Camp, H. J. M. O. den. Rare Earth Metals Are Essential for Methanotrophic Life in Volcanic Mudpots. *Environmental Microbiology* **2014**, *16* (1), 255–264. https://doi.org/10.1111/1462-2920.12249.
(36) Keltjens, J. T.; Pol, A.; Reimann, J.; Op den Camp, H. J. M. PQQ-Dependent Methanol Dehydrogenases: Rare-Earth Elements Make a Difference. *Appl Microbiol Biotechnol* **2014**, *98* (14), 6163–6183. https://doi.org/10.1007/s00253-014-5766-8.
(37) Huang, J.; Yu, Z.; Groom, J.; Cheng, J.-F.; Tarver, A.; Yoshikuni, Y.; Chistoserdova, L. Rare Earth Element Alcohol Dehydrogenases Widely Occur among Globally Distributed, Numerically Abundant

and Environmentally Important Microbes. *ISME J* **2019**, *13* (8), 2005–2017. https://doi.org/10.1038/s41396-019-0414-z.
(38) Mattocks, J. A.; Ho, J. V.; Cotruvo, J. A. Jr. A Selective, Protein-Based Fluorescent Sensor with Picomolar Affinity for Rare Earth Elements. *J. Am. Chem. Soc.* **2019**, *141* (7), 2857–2861. https://doi.org/10.1021/jacs.8b12155.
(39) Cotruvo, J. A. Jr.; Featherston, E. R.; Mattocks, J. A.; Ho, J. V.; Laremore, T. N. Lanmodulin: A Highly Selective Lanthanide-Binding Protein from a Lanthanide-Utilizing Bacterium. *J. Am. Chem. Soc.* **2018**, *140* (44), 15056–15061. https://doi.org/10.1021/jacs.8b09842.
(40) Chistoserdova, L. New Pieces to the Lanthanide Puzzle. *Molecular Microbiology* **2019**, *111* (5), 1127–1131. https://doi.org/10.1111/mmi.14210.
(41) Wegner, C.-E.; Gorniak, L.; Riedel, S.; Westermann, M.; Küsel, K. Lanthanide-Dependent Methylotrophs of the Family Beijerinckiaceae: Physiological and Genomic Insights. *Applied and Environmental Microbiology* **2019**, *86* (1), e01830-19. https://doi.org/10.1128/AEM.01830-19.
(42) Masuda, S.; Suzuki, Y.; Fujitani, Y.; Mitsui, R.; Nakagawa, T.; Shintani, M.; Tani, A. Lanthanide-Dependent Regulation of Methylotrophy in Methylobacterium Aquaticum Strain 22A. *mSphere* **2018**, *3* (1), e00462-17. https://doi.org/10.1128/mSphere.00462-17.
(43) Roszczenko-Jasińska, P.; Vu, H. N.; Subuyuj, G. A.; Crisostomo, R. V.; Cai, J.; Lien, N. F.; Clippard, E. J.; Ayala, E. M.; Ngo, R. T.; Yarza, F.; Wingett, J. P.; Raghuraman, C.; Hoeber, C. A.; Martinez-Gomez, N. C.; Skovran, E. Gene Products and Processes Contributing to Lanthanide Homeostasis and Methanol Metabolism in Methylorubrum Extorquens AM1. *Sci Rep* **2020**, *10* (1), 12663. https://doi.org/10.1038/s41598-020-69401-4.
(44) Cook, E. C.; Featherston, E. R.; Showalter, S. A.; Cotruvo, J. A. Jr. Structural Basis for Rare Earth Element Recognition by *Methylobacterium Extorquens* Lanmodulin. *Biochemistry* **2019**, *58* (2), 120–125. https://doi.org/10.1021/acs.biochem.8b01019.
(45) Deblonde, G. J.-P.; Mattocks, J. A.; Park, D. M.; Reed, D. W.; Cotruvo, J. A.; Jiao, Y. Selective and Efficient Biomacromolecular Extraction of Rare-Earth Elements Using Lanmodulin. *Inorg. Chem.* **2020**, *59* (17), 11855–11867. https://doi.org/10.1021/acs.inorgchem.0c01303.
(46) Deblonde, G.; Mattocks, J. A.; Dong, Z.; Wooddy, P. T.; Cotruvo; Zavarin, M. Protein-Based Platform for Purification, Chelation, and Study of Medical Radiometals: Yttrium and Actinium. *ChemRxiv* **2021**. https://doi.org/10.26434/chemrxiv.14763426.v1.
(47) Xu, C.; Santschi, P. H.; Zhong, J. Y.; Hatcher, P. G.; Francis, A. J.; Dodge, C. J.; Roberts, K. A.; Hung, C.-C.; Honeyman, B. D. Colloidal Cutin-Like Substances Cross-Linked to Siderophore Decomposition Products Mobilizing Plutonium from Contaminated Soils. *Environ. Sci. Technol.* **2008**, *42* (22), 8211–8217. https://doi.org/10.1021/es801348t.
(48) Boggs, M. A.; Mason, H.; Arai, Y.; Powell, B. A.; Kersting, A. B.; Zavarin, M. Nuclear Magnetic Resonance Spectroscopy of Aqueous Plutonium(IV) Desferrioxamine B Complexes. *European Journal of Inorganic Chemistry* **2014**, *2014* (21), 3312–3321. https://doi.org/10.1002/ejic.201402105.
(49) Boukhalfa, H.; Reilly, S. D.; Neu, M. P. Complexation of Pu(IV) with the Natural Siderophore Desferrioxamine B and the Redox Properties of Pu(IV)(Siderophore) Complexes. *Inorg. Chem.* **2007**, *46* (3), 1018–1026. https://doi.org/10.1021/ic061544q.
(50) Grimes, T. S.; Heathman, C. R.; Jansone-Popova, S.; Ivanov, A. S.; Bryantsev, V. S.; Zalupski, P. R. Exploring Soft Donor Character of the N-2-Pyrazinylmethyl Group by Coordinating Trivalent Actinides and Lanthanides Using Aminopolycarboxylates. *Inorg. Chem.* **2020**, *59* (1), 138–150. https://doi.org/10.1021/acs.inorgchem.9b01427.
(51) Grimes, T. S.; Heathman, C. R.; Jansone-Popova, S.; Bryantsev, V. S.; Goverapet Srinivasan, S.; Nakase, M.; Zalupski, P. R. Thermodynamic, Spectroscopic, and Computational Studies of f-

Element Complexation by N-Hydroxyethyl-Diethylenetriamine-N,N',N",N"-Tetraacetic Acid. *Inorg. Chem.* **2017**, *56* (3), 1722–1733. https://doi.org/10.1021/acs.inorgchem.6b02897.
(52) Sperling, J. M.; Warzecha, E.; Klamm, B. E.; Gaiser, A. N.; Windorff, C. J.; Whitefoot, M. A.; Albrecht-Schönzart, T. E. Pronounced Pressure Dependence of Electronic Transitions for Americium Compared to Isomorphous Neodymium and Samarium Mellitates. *Inorg. Chem.* **2021**, *60* (1), 476–483. https://doi.org/10.1021/acs.inorgchem.0c03293.
(53) Özçubukçu, S.; Mandal, K.; Wegner, S.; Jensen, M. P.; He, C. Selective Recognition of Americium by Peptide-Based Reagents. *Inorg. Chem.* **2011**, *50* (17), 7937–7939. https://doi.org/10.1021/ic201094e.
(54) Featherston, E. R.; Issertell, E. J.; Cotruvo, J. A. Jr. Probing Lanmodulin's Lanthanide Recognition via Sensitized Luminescence Yields a Platform for Quantification of Terbium in Acid Mine Drainage. *J. Am. Chem. Soc.*, accepted.
(55) Runde, W. H.; Schulz, W. W. Americium. In *The Chemistry of the Actinide and Transactinide Elements*; Morss, L. R., Edelstein, N. M., Fuger, J., Eds.; Springer Netherlands: Dordrecht, 2006; pp 1265–1395. https://doi.org/10.1007/1-4020-3598-5_8.
(56) Leguay, S.; Vercouter, T.; Topin, S.; Aupiais, J.; Guillaumont, D.; Miguirditchian, M.; Moisy, P.; Le Naour, C. New Insights into Formation of Trivalent Actinides Complexes with DTPA. *Inorg. Chem.* **2012**, *51* (23), 12638–12649. https://doi.org/10.1021/ic3011019.
(57) Lapka, J. L.; Wahu, S.; Sinkov, S.; Nash, K. L. Ternary Complex Formation and Extraction Modeling in Malonate-Buffered Trivalent Actinide–Lanthanide Separations. *Inorg. Chem.* **2019**, *58* (11), 7554–7563. https://doi.org/10.1021/acs.inorgchem.9b00808.
(58) Zavarin, M.; Powell, B. A.; Bourbin, M.; Zhao, P.; Kersting, A. B. Np(V) and Pu(V) Ion Exchange and Surface-Mediated Reduction Mechanisms on Montmorillonite. *Environ. Sci. Technol.* **2012**, *46* (5), 2692–2698. https://doi.org/10.1021/es203505g.
(59) Peters, A. J.; Hamilton-Taylor, J.; Tipping, E. Americium Binding to Humic Acid. *Environ. Sci. Technol.* **2001**, *35* (17), 3495–3500. https://doi.org/10.1021/es000295g.
(60) Yoshida, Z.; Johnson, S. G.; Kimura, T.; Krsul, J. R. Neptunium. In *The Chemistry of the Actinide and Transactinide Elements*; Morss, L. R., Edelstein, N. M., Fuger, J., Eds.; Springer Netherlands: Dordrecht, 2006; pp 699–812. https://doi.org/10.1007/1-4020-3598-5_6.
(61) Griffiths, T. L.; Martin, L. R.; Zalupski, P. R.; Rawcliffe, J.; Sarsfield, M. J.; Evans, N. D. M.; Sharrad, C. A. Understanding the Solution Behavior of Minor Actinides in the Presence of EDTA4–, Carbonate, and Hydroxide Ligands. *Inorg. Chem.* **2013**, *52* (7), 3728–3737. https://doi.org/10.1021/ic302260a.
(62) Johnson, S. G. *NIST46 - NIST Critically Selected Stability Constants of Metal Complexes:*; Standard Reference Data Program; National Institute of Standards and Technology: Gaithersburg, MD. USA, 2013.
(63) Lundberg, D.; Persson, I. The Size of Actinoid(III) Ions – Structural Analysis vs. Common Misinterpretations. *Coordination Chemistry Reviews* **2016**, *318*, 131–134. https://doi.org/10.1016/j.ccr.2016.04.003.
(64) Bauer, N.; Panak, P. J. Influence of Carbonate on the Complexation of Cm(III) with Human Serum Transferrin Studied by Time-Resolved Laser Fluorescence Spectroscopy (TRLFS). *New J. Chem.* **2015**, *39* (2), 1375–1381. https://doi.org/10.1039/C4NJ01877J.
(65) Thakur, P.; Conca, J. L.; Van De Burgt, L. J.; Choppin, G. R. Complexation and the Laser Luminescence Studies of Eu(III), Am(III), and Cm(III) with EDTA, CDTA, and PDTA and Their Ternary Complexation with Dicarboxylates. *Journal of Coordination Chemistry* **2009**, *62* (23), 3719–3737. https://doi.org/10.1080/00958970903183909.
(66) Alderighi, L.; Gans, P.; Ienco, A.; Peters, D.; Sabatini, A.; Vacca, A. Hyperquad Simulation and Speciation (HySS): A Utility Program for the Investigation of Equilibria Involving Soluble and

Partially Soluble Species. *Coordination Chemistry Reviews* **1999**, *184* (1), 311–318. https://doi.org/10.1016/S0010-8545(98)00260-4.
(67) Lumetta, G. J.; Thompson, M. C.; Penneman, R. A.; Eller, P. G. Curium. In *The Chemistry of the Actinide and Transactinide Elements*; Morss, L. R., Edelstein, N. M., Fuger, J., Eds.; Springer Netherlands: Dordrecht, 2006; pp 1397–1443. https://doi.org/10.1007/1-4020-3598-5_9.
(68) Kimura, T.; Choppin, G. R.; Kato, Y.; Yoshida, Z. Determination of the Hydration Number of Cm(III) in Various Aqueous Solutions. *Radiochimica Acta* **1996**, *72* (2), 61–64. https://doi.org/10.1524/ract.1996.72.2.61.
(69) Boros, E.; Polasek, M.; Zhang, Z.; Caravan, P. Gd(DOTAla): A Single Amino Acid Gd-Complex as a Modular Tool for High Relaxivity MR Contrast Agent Development. *J. Am. Chem. Soc.* **2012**, *134* (48), 19858–19868. https://doi.org/10.1021/ja309187m.
(70) Gale, E. M.; Kenton, N.; Caravan, P. [Gd(CyPic3A)(H2O)2]−: A Stable, Bis(Aquated) and High-Relaxivity Gd(III) Complex. *Chem. Commun.* **2013**, *49* (73), 8060–8062. https://doi.org/10.1039/C3CC44116D.
(71) Boros, E.; Caravan, P. Probing the Structure–Relaxivity Relationship of Bis-Hydrated Gd(DOTAla) Derivatives. *Inorg. Chem.* **2015**, *54* (5), 2403–2410. https://doi.org/10.1021/ic503035f.
(72) Caravan, P.; Parigi, G.; Chasse, J. M.; Cloutier, N. J.; Ellison, J. J.; Lauffer, R. B.; Luchinat, C.; McDermid, S. A.; Spiller, M.; McMurry, T. J. Albumin Binding, Relaxivity, and Water Exchange Kinetics of the Diastereoisomers of MS-325, a Gadolinium(III)-Based Magnetic Resonance Angiography Contrast Agent. *Inorg. Chem.* **2007**, *46* (16), 6632–6639. https://doi.org/10.1021/ic700686k.
(73) Vu, H. N.; Subuyuj, G. A.; Vijayakumar, S.; Good, N. M.; Martinez-Gomez, N. C.; Skovran, E. Lanthanide-Dependent Regulation of Methanol Oxidation Systems in Methylobacterium Extorquens AM1 and Their Contribution to Methanol Growth. *Journal of Bacteriology* **2016**, *198* (8), 1250–1259. https://doi.org/10.1128/JB.00937-15.
(74) Whisenhunt, Donald W.; Neu, M. P.; Hou, Z.; Xu, J.; Hoffman, D. C.; Raymond, K. N. Specific Sequestering Agents for the Actinides. 29. Stability of the Thorium(IV) Complexes of Desferrioxamine B (DFO) and Three Octadentate Catecholate or Hydroxypyridinonate DFO Derivatives: DFOMTA, DFOCAMC, and DFO-1,2-HOPO. Comparative Stability of the Plutonium(IV) DFOMTA Complex1. *Inorg. Chem.* **1996**, *35* (14), 4128–4136. https://doi.org/10.1021/ic951064r.
(75) Codd, R.; Richardson-Sanchez, T.; Telfer, T. J.; Gotsbacher, M. P. Advances in the Chemical Biology of Desferrioxamine B. *ACS Chem. Biol.* **2018**, *13* (1), 11–25. https://doi.org/10.1021/acschembio.7b00851.
(76) Bellotti, D.; Remelli, M. Deferoxamine B: A Natural, Excellent and Versatile Metal Chelator. *Molecules* **2021**, *26* (11), 3255. https://doi.org/10.3390/molecules26113255.
(77) Morrison, K. D.; Jiao, Y.; Kersting, A. B.; Zavarin, M. Reduction of Plutonium(VI) to (V) by Hydroxamate Compounds at Environmentally Relevant PH. *Environ. Sci. Technol.* **2018**, *52* (11), 6448–6456. https://doi.org/10.1021/acs.est.8b00164.
(78) Moll, H.; Glorius, M.; Bernhard, G. Curium(III) Complexation with Desferrioxamine B (DFO) Investigated Using Fluorescence Spectroscopy. *BCSJ* **2008**, *81* (7), 857–862. https://doi.org/10.1246/bcsj.81.857.
(79) Christenson, E. A.; Schijf, J. Stability of YREE Complexes with the Trihydroxamate Siderophore Desferrioxamine B at Seawater Ionic Strength. *Geochimica et Cosmochimica Acta* **2011**, *75* (22), 7047–7062. https://doi.org/10.1016/j.gca.2011.09.022.
(80) Adam, Z. Actinides and Life's Origins. *Astrobiology* **2007**, *7* (6), 852–872. https://doi.org/10.1089/ast.2006.0066.
(81) Helland, R.; Fjellbirkeland, A.; Karlsen, O. A.; Ve, T.; Lillehaug, J. R.; Jensen, H. B. An Oxidized Tryptophan Facilitates Copper Binding in Methylococcus Capsulatus-Secreted Protein MopE *.

Journal of Biological Chemistry **2008**, *283* (20), 13897–13904. https://doi.org/10.1074/jbc.M800340200.
(82) Kenney, G. E.; Rosenzweig, A. C. Chalkophores. *Annu. Rev. Biochem.* **2018**, *87* (1), 645–676. https://doi.org/10.1146/annurev-biochem-062917-012300.
(83) Mattocks, J. A.; Tirsch, J. L.; Cotruvo, J. A. Chapter Two - Determination of Affinities of Lanthanide-Binding Proteins Using Chelator-Buffered Titrations. In *Methods in Enzymology*; Cotruvo, J. A., Ed.; Rare-Earth Element Biochemistry: Characterization and Applications of Lanthanide-Binding Biomolecules; Academic Press, 2021; Vol. 651, pp 23–61. https://doi.org/10.1016/bs.mie.2021.01.044.
(84) Deblonde, G. J.-P. Spectrophotometric Methods to Probe the Solution Chemistry of Lanthanide Complexes with Macromolecules. In *Methods in Enzymology*; Academic Press, 2021. https://doi.org/10.1016/bs.mie.2020.12.012.
(85) Gale, E. M.; Zhu, J.; Caravan, P. Direct Measurement of the Mn(II) Hydration State in Metal Complexes and Metalloproteins through 17O NMR Line Widths. *J. Am. Chem. Soc.* **2013**, *135* (49), 18600–18608. https://doi.org/10.1021/ja4094132.
(86) Caravan, P.; Astashkin, A. V.; Raitsimring, A. M. The Gadolinium(III)−Water Hydrogen Distance in MRI Contrast Agents. *Inorg. Chem.* **2003**, *42* (13), 3972–3974. https://doi.org/10.1021/ic034414f.

Acknowledgments

This work was performed under the auspices of the U.S. Department of Energy (DOE) by Lawrence Livermore National Laboratory under Contract DE-AC52-07NA27344 (LLNL-JRNL-824360). G.J.-P.D. acknowledges the LLNL-LDRD program, project No. 20-LW-017. J.A.M. and J.A.C. were supported by DOE grant DE-SC0021007. H.W. and E.M.G. were supported by grants from the National Institute of Diabetes and Digestive and Kidney Diseases (R01DK120663) and the National Heart, Lung, and Blood Institute (K25HL128899), as well as instrumentation funded by the Office of the Director (ODS10025234).

Author Information

*Corresponding Authors: Deblonde1@LLNL.gov (G.J.-P.D.) and juc96@psu.edu (J.A.C.)

Competing interests

The authors declare the following competing financial interests: G.J.-P.D., J.A.M., and J.A.C. are listed as inventors on patent applications submitted by Lawrence Livermore National Laboratory and the Pennsylvania State University.

Supporting Information

Supplemental figures and tables including additional thermodynamic, spectrophotometric, and luminescence characterization of LanM's complexes with Am^{3+} and Cm^{3+}; Am/Np separation data; temperature-dependence ^{17}O NMR data; Cm^{3+}-LanM/DFOB competition experiments. Supplemental tables including stability constants and pK_a values of metal ion complexes relevant to this work.

FOR TABLE OF CONTENTS USE ONLY